N71-19164   *K*

MTI-70TR16

DYNAMICAL ANALYSIS OF NON-EQUILIBRIUM
FORCED CONVECTIVE BOILING FLOWS

by

C.H.T. Pan
J. H. Vohr

December 1970

MTI   ... research and development division

MTI-70TR16

DYNAMICAL ANALYSIS OF NON-EQUILIBRIUM
FORCED CONVECTIVE BOILING FLOWS

by

C.H.T. Pan
J. H. Vohr

December 1970

TECHNICAL REPORT

DYNAMICAL ANALYSIS OF NON-EQUILIBRIUM
FORCED CONVECTIVE BOILING FLOWS

by

C.H.T. Pan
J. H. Vohr

Author (s)

Approved

Approved

Prepared for

NASA Headquarters
Washington, D. C.

Prepared under

Contract No. NASw-1705

MTI
MECHANICAL TECHNOLOGY INCORPORATED

FOREWORD

The work described in this report was performed by Mechanical Technology Incorporated under NASA Contract NASw-1705. The overall objective of this contract was to develop a comprehensive dynamical theory of forced-convection boiling in liquid metals. This is the Final Technical Report of the subject contract, containing a summary of all essential results obtained in the contract work.

The work was done under the technical management of Mr. S. V. Manson, NASA Headquarters, Nuclear Power Systems.

TABLE OF CONTENTS

INTRODUCTION

The combination of excellent thermal conductivity, high vaporization temperature and moderate vapor pressure possessed by alkali metals makes them very attractive for use as working fluids for Rankine cycle space power systems. Consequently, considerable effort has been devoted recently toward development of once-through alkali metal boilers in which the liquid metal enters subcooled, is vaporized and departs as saturated or superheated vapor. Much of the work to date has concentrated on boilers for potassium and sodium, and considerable attention has been paid to the problem of achieving stability of operation of such boilers.

A number of traditional instability mechanisms for boiling flow have been recognized for some time, e.g. "Ledinegg Excursions," and liquid metal boilers are subject to these instabilities as well as are water boilers. The problem of the stability of liquid metal boilers, however, is further complicated by the fact that liquid metals can exhibit very large degrees of superheating before inception of boiling. This makes dynamic analysis of boiling liquid metal flow quite difficult because one can no longer assume that the flow is in thermodynamic equilibrium. Moreover, the superheating of liquid metals appear to give rise to a unique type of flow instability associated with drastic flow regime changes in the boiling channel. This instability is of the following nature.

When power input to the heated length of a liquid metal boiler is steadily increased from zero, a point is reached when the flow temperature at the exit of the heated length reaches saturation temperature. Due to the tendency of liquid metals to superheat in the liquid phase, further increase in power often does not result in inception of boiling, but rather leads to the condition that superheated flow exits from the heated length. As power is further increased, however, a point is reached where the degree of superheat, θ, at the exit is sufficiently large such that nucleation of vapor bubbles will occur and boiling will commence. The boiling will then tend to propagate upstream into superheated liquid, causing a sudden change of flow regimes and resulting in undesirable rapid temperature fluctuations in the boiling channel. The vapor liquid interface then can (a) reach a stable position, (b) oscillate within a finite zone, or (c) be swept back

out of the boiler to reenter later as superheating again accumulates. The latter two modes are, of course, deemed unstable and are to be avoided if possible. Which mode occurs is governed by the thermo-hydraulic characteristics of the boiler and its associated flow loop.

Because of the technological importance of liquid metal boilers an analytical program was undertaken at M.T.I. under NASA Contract Number NASw-1705 directed toward obtaining solutions for the thermo-hydraulic liquid metal boiler stability problem. The crux of this study is the problem of the non-equilibrium behavior of liquid metal flows.

The program was carried out in two phases. The first phase is concerned with the prediction of incipient boiling, and the corresponding study has been documented in a topical report. MTI-69TR45, "A Review of Criteria for Predicting Incipient Nucleation in Liquid Metals and Ordinary Fluids," by J.H. Vohr and T. Chiang [1].

The second phase is concerned with the determination of vaporization rates for each of various relevant flow regimes. Emphasis is placed on the release of liquid superheat with the attendant generation of the vapor phase, since the substantial change in density would cause pressure rise and consequently would be a principal driving force for the dynamic motion in a thermo-hydraulic system. The specific analyses on various mechanisms of evaporation are then recast in terms of a vapor generation rate which represents the constitutive relation of the evaporative process. This study culminated in a second topical report, MTI-70TR15, "Evaporation Processes in Superheated Forced Convective Boiling," by J.H. Vohr, [29].

This document is the Final Technical Report of the subject contract. It contains a comprehensive digest of the two topical reports, including the essential formulae, graphical results, and citations of the original sources. The substance of the first topical report is contained in the chapter entitled, "Criteria for Incipient Nucleation for Boiling", that of the second topical report is contained in the chapter entitled "Void Growth and Evaporation Rate".

Since the subject matter is a rapidly developing technology, a discussion is provided on areas where basic knowledge is still lacking and avenues for furthering needed progress are suggested.

CRITERIA FOR INCIPIENT NUCLEATION FOR BOILING

A review of the subject was made by compiling available experimental evidence
and by discussing the basic foundations underlying the current understanding
of various physical parameters governing the correlation of experimental data.
The study was begun by Dr. D. E. Dougherty and completed by Drs. J. H. Vohr
and T. Chiang who are identified as co-authors of the topical report [1].
Dr. John Chen of Brookhaven National Laboratory, who was retained as a con-
sultant to this project, contributed substantially to the collection of pub-
lished experimental data and their interpretations.

The principal premise of the study attributes the boiling nucleation process
to be dominated by sites present on the boiler walls as surface cavities. The
need of superheating to initiate nucleation is presumed to be the requirement
for a pressure excess abpve the saturation vapor pressure in the cavities to
overcome the surface tension of the liquid. That is, for incipient boiling
nucleation to take place, a lower bound of the vapor pressure is, Eq. (3) of
[1]:

$$P_v = P - P_g + 2\sigma/r \tag{1}$$

where,

P_v = vapor pressure in the cavity

P = system pressure

P_g = partial pressure of inert gas in the cavity

σ = surface tension of liquid at saturation temperature corresponding
to P

r = bubble radius of nucleating cavity.

The required superheat is related to P_v - P along the saturation line of the
fluid in question, or according to the Clausius-Clapeyron equation.

$$\frac{dP_{sat}}{dT_{sat}} = \frac{h_{fg}}{T_{sat}(v_v - v_\ell)}$$

where

h_{fg} = latent heat of vaporization at T_{sat}

v_v = specific volume of vapor phase

v_ℓ = specific volume of liquid phase, and

the subscripts "sat" refer to the saturation state. Available experimental data on boiling incipience were analyzed and correlated in relation to interpretations of the bubble radius r and the reference temperature T.

From twenty-one reported investigations [2-22], experimental data on the boiling incipience of alkali metals were critically reviewed. A summary of the significant findings of these investigations is given in Table I. Because of the good thermal conductivity of liquid metals, temperature variations in the immediate vicinity of nucleation sites are believed to be negligible. The major parameters governing the magnitude of incipience superheat are identified as the system pressure and deactivation history. The available experimental data on the effect of deactivation history can be interpreted according to alternative postulated detail mechanisms regarding penetration of liquid into surface cavities. The Holtz-Chen-Dwyer model required penetration of liquid into nucleation sites to be terminated at a non-wetting condition and the presence of non-condensible gas being compressed by the deactivating pressure inside cavities of conical shape. The re-entrant cavity model allows the nucleation sites not to become completely flooded by a wetting liquid by geometrical arguments.

To check the plausibility of the actual existence of surface pits or cavities which would function as nucleation sites at the incipience of boiling according to the mechanisms postulated above, sections of SS 347 tubings were examined under 750 X magnification. Samples were made from both seamless extruded and welded tubings. Typical photo-micrographs are shown in Figs. 1 and 2. Pits less than 0.2 mil in overall dimension would not be discernible. All pits found were less than 0.6 mil at their mouths. They are classified into five geometrical types, as shown in Table II. The population density of pits found on the welded tubing was about 2-3.5 times those found on the seamless extruded tubing; otherwise the different methods of fabrication do not seem to have caused much difference in the surface

TABLE I   Summary of Experimental Investigations of Boiling and Incipient Nucleation Superheat for Alkali Liquid Metals

REFERENCE	AUTHORS	TEST FLUIDS	SYSTEM	INCIPIENT θ_{inc} (°F)	BOILING SUPERHEAT (°F)	PRESSURE (PSIA)	VARIABLES INVESTIGATED	RESULTS AND COMMENTS
2	Edwards and Hoffman	K Na	Natural convection loop		K: 2°-500° Na: 50°-700°	0.8-65	(1) Boiling pressure (T_{sat}) (2) Surface finish - artificial cavities	θ_{inc} measured under cyclic temperature fluctuations associated with periodic natural convection flow. Artificial cavities significantly reduced θ_{inc}.
3	Edwards and Hoffman	K	Natural convection loop	90°-500°	6°-80°	1-40	(1) Boiling pressure (T_{sat}) (2) Artificial re-entrant cavities	Incipient θ_{inc} measured under transient heat-up conditions. Incipient θ_{inc} are consistently greater than "stable" boiling superheat. Re-entrant cavities are about as effective in reducing θ_{inc} as cylindrical cavities of same size.
4	Holtz and Singer	Na	Pool (in 2" diameter pipe)	40°-280°		0.2-15	(1) Boiling pressure (T_{sat}) (2) Heat flux (low level) (3) Deactivation pressure (4) Pressure pulses during boiling	θ_{inc} measured under transient heat-up. Increasing pressure gives lower incipient θ_{inc} and greater probability for stable sustained boiling. In this low heat flux range (< 20,000 $\frac{Btu}{hr-ft^2}$) incipient θ_{inc} found to increase with increasing heat flux. Possibility of inadvertent nucleation at "rogue" sites outside of polished test zone – combining with transient heating to give seeming effect of heat flux on θ_{inc}.
5	Holtz and Singer	Na	Pool (same as Reference 4)	40°-300°		0.2-15	same as Reference 4	Essentially the same study as Reference 4, but gives more plots of experimental results. Definite deactivation pressure affect, though measured θ_{inc} were very much lower (by factor of ~ 2 to ~ 50) than predicted by Holtz's "previous history" model. Same question of "rogue" sites as in Reference 4.
6	Marto and Rohsenow	Na	Pool-boiling off horizontal	20°-130°	2°-60°	1-8	(1) Boiling pressure (2) Heat flux, up to 236,000 $\frac{Btu}{hr-ft^2}$ (3) Surface finish-artificial cavities, porous welds, etc.	Higher incipient θ_{inc} than stable-boiling superheat shown on standard boiling curve. Strong effect of surface finish. Noticeable hysterisis or "history" effect.
7 8	Lurie and Noyes	Na	Pool and forced convection in		Pool: 20°-60° Forced-Convection 30°-80°	2-5	(1) Boiling pressure (2) Bulk subcooling (3) Heat flux	Primarily offer steady boiling and critical heat flux data. Pool boiling results for well superheat in fair agreement with Freta-Zuber correlation. Convective boiling, with bulk subcooling had incipient boiling essentially coincide with critical heat flux (at fluxes ~10^6 $\frac{Btu}{hr-ft^2}$.
9	Petukhov, Kovalev,	Na	Pool boiling on horizontal rod	~ 30°-300°		0.15-12	(1) Heat flux (2) Boiling pressure	Primarily after pool boiling heat transfer data. Observed temperature fluctuations associated with periodic changes between natural convection heat transfer and bumping of boiling
10 11	Shae and Rohsenow	Na	Pool boiling off horizontal surface	Up to 150°F	20°-100°	1-2	(1) Heat flux (2) Artificial cavities (3) Boiling pressure	Traces for a thermocouple near boiling surfaces showed temperature fluctuations of ~80°F for bumping boiling versus ~100°F for stable-boiling. Boiling superheat of ~100°F obtained with natural convection heat transfer at heat flux of ~80,000. This drops to ~25°F on start of bumping-boiling. Even during stable-boiling the boiling superheat from extrapolated temperature measured within solid was~ 30°F less than boiling superheat corresponding to maximum surface temperature measured by "surface thermocouple" in temperature cycling.

MTI-7981

TABLE I (Continued)

| REFERENCE	AUTHORS	TEST FLUIDS	SYSTEM	INCIPIENT θ_{inc} (°F)	BOILING SUPERHEAT (°F)	PRESSURE (PSIA)	VARIABLES INVESTIGATED	RESULTS AND COMMENTS
12	Chen	K	Forced convection loop	17°-117°		8-24	(1) Boiling pressure (2) Pre-boiling deactivation condition	Data indicated significant dependence of θ_{inc} for incipient vaporization on deactivation temperature, deactivation pressure, and boiling pressure boiling inception obtained after controlled deactivation by small incremental increases in heat flux (and fluid temperature). Flow maintained constant at ~ 0.2 ft/sec.
13	Logan et.al.	Na	Forced convection loop	bulk θ_{inc} -14° to 100°		8-12	(1) Heat flux (2) Boiling pressure (3) Flow velocity	Large random scatter in measured θ_{inc}. The maximum bulk θ_{inc} seemed to increase with heat flux and to decrease with velocity.
14	Bond and Converse	K	Forced convection loop		mostly 50°		(1) Boiling pressure (2) Heat flux (3) Flow quality	T_{sat} was taken to be that corresponding to exit pressure. Therefore, θ_{inc} actual, based on local true local T_{sat} would be less than the reported values.
15	Grass et.al.	K Na	Stagnant, natural convection and convection in tube	40°-1500°		1-7	(1) Boiling pressure (2) Duration of tests (3) Flowing versus	Heating by electric resistance in tube wall and in liquid metal. Large scatter in θ_{inc} results with a Goussian type of distribution about a most probable value of θ_{inc}, for a given set of conditions. Contrary to theory, found θ_{inc} higher for K than for Na. Flow conditions gives "slightly" lower θ_{inc} than stagnant conditions. Measured θ_{inc} increased with number of days of operating time.
16	LeGonidec et.al.	Na	Stagnant pool in tube	40°-320°		1-20	(1) Boiling pressure (2) Duration of operation (3) Heating power	Tests used transient heating by electrical resistance through tube. Almost 1 order of magnitude in scatter of data. θ_{inc} does show decrease with increasing pressure. Report θ_{inc} increase with duration of operation. No noticeable effect of heating power.
17	Pinchera et.al.	Na	Heat rod in pool and forced convection	0°-300°		1.5-15	(1) Boiling pressure (2) Flow velocity	Stagnant Na tests shown θ_{inc} spread ≈ 100°-300°, with no clear dependence on pressure. Flow θ_{inc} decreased from ≈ 170°F (max) to 18°F (min) as velocity changed from 0.4 to 1.6 m/sec.
18	Pinchera et.al.	Na	Capsule	10°-140°	12°-25°	1.7-15	(1) Boiling pressure (2) Heat flux (3) Transient heating versus steady boiling	Wide scatter for θ_{inc} obtained with transient heating; e.g. at T of 780°C, θ_{inc} varied 10°F to 100°F. For steady boiling, at a given heat flux, boiling superheat decreased as T_{sat} increased (up to 830°C). The boiling curves show marked hysterisis due to incipient-boiling superheating.
19	Smidt et.al.	Na	Capsule	100°-500°		1-15	(1) Boiling pressure (2) Na purity	Results in this report obrained by slowly decreasing pressure in the capsule. Data show good precision. θ_{inc} correspond to calculated cavity radii of 1-5μ.
20	Logan et.al.	Na	Forced convection loop	0°-140°			(1) Flow velocity (2) Surface finish	For a given flow rate, θ_{inc} scattered about a mean value. The mean θ_{inc} decreased with increasing flow velocity.
21	Chen	K	Forced convection loop	10°-120°		24-8	(1) Flow rate (2) Boiling pressure (3) Deactivation condition	At any constant deactivation and boiling pressure, θ_{inc} showed definite parametric dependence on flow rate, decreasing with increasing flow. Theoretical explanation is proposed, based on turbulent pressure fluctuations.
22	Holtz	Na	Pool	Up to 200°		15	(1) Deactivation condition (2) Boiling pressure (3) Surface roughness (4) Neutron flux	Verified the strong effect of deactivation history. Deactivation effect over-rides effect of gross variations in surface roughness. Earlier heat flux effect explained in terms of gas diffusion. Increased oxide concentration decreases θ_{inc}. No discernible effect from neutron (thermal level) flux.
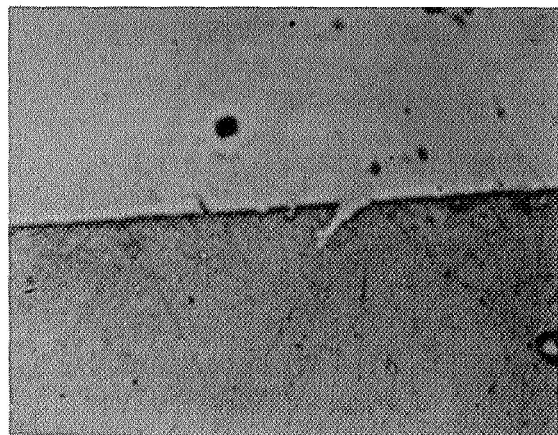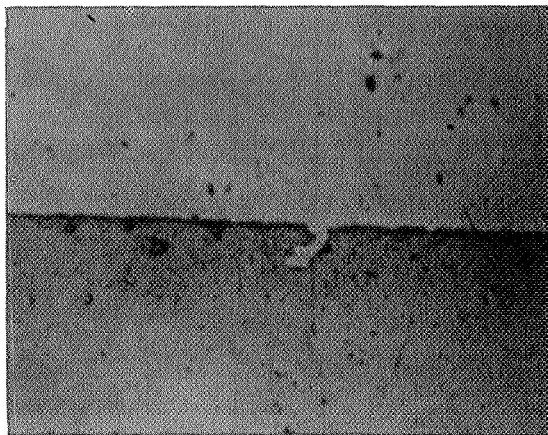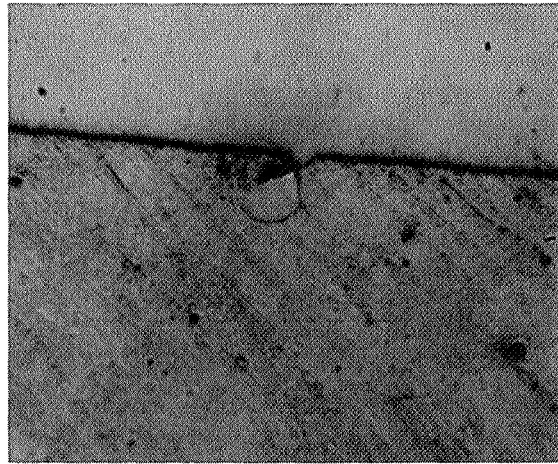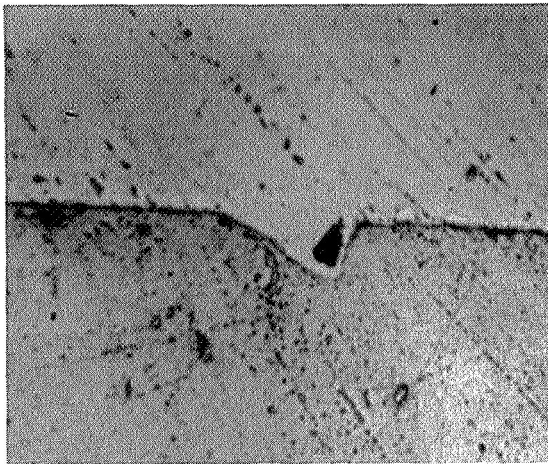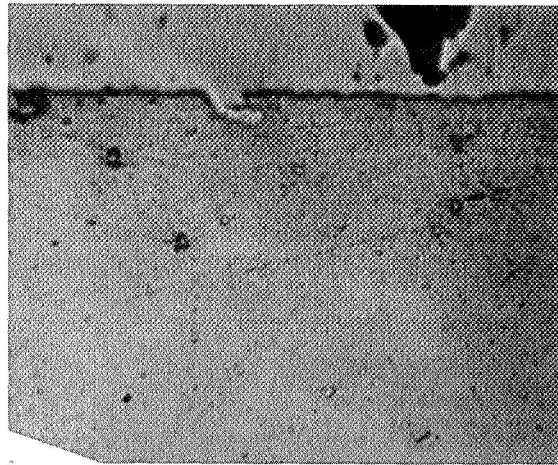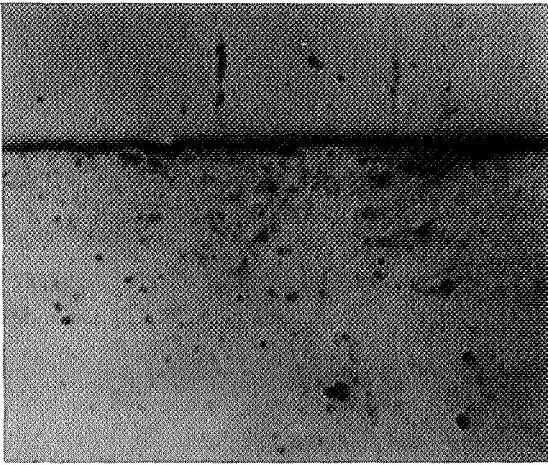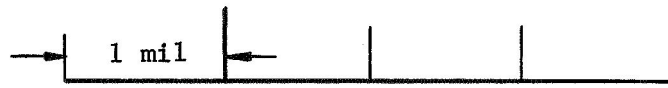
Fig. 1   Photomicrographs of Seamless Tubing Made of 347SS, with
3/8" O.D. and 35 mil. Wall Thickness.

1 mil
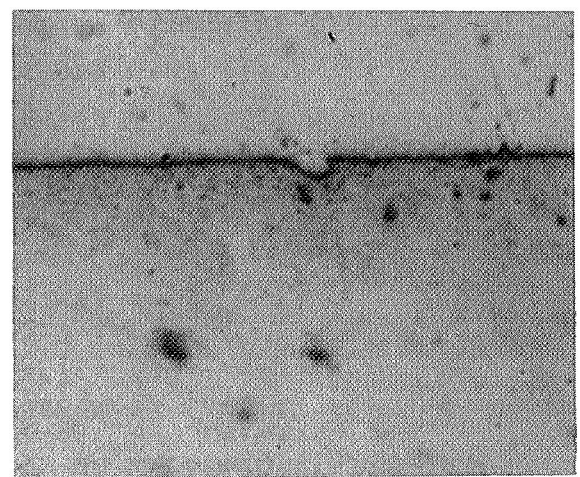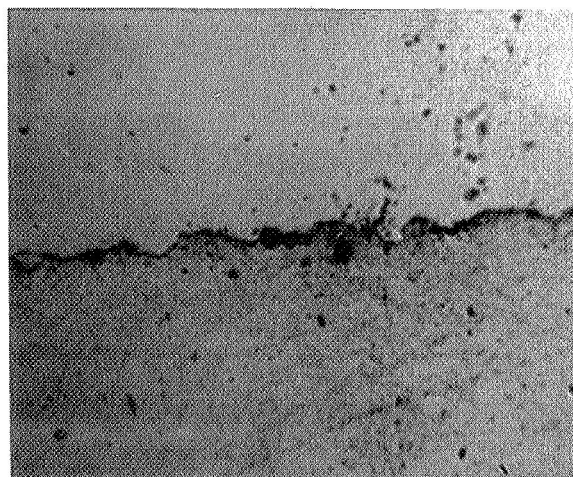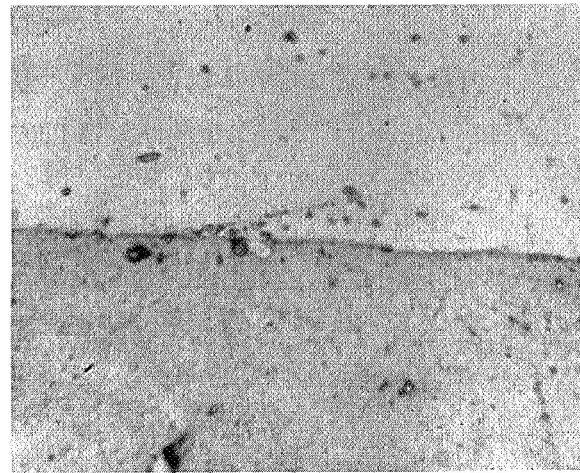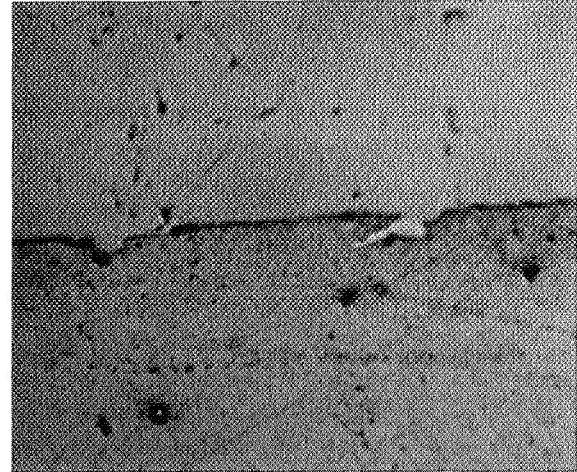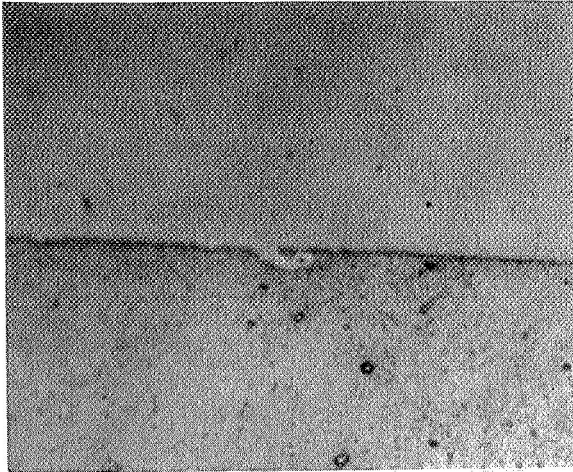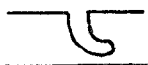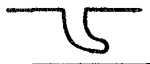
Fig. 2   Photomicrographs of Welded Tubing Made of 347 SS, with
3/8" O.D. and 35 mil. Wall Thickness

MTI–5764

TABLE II

Number of Pits at O.D.
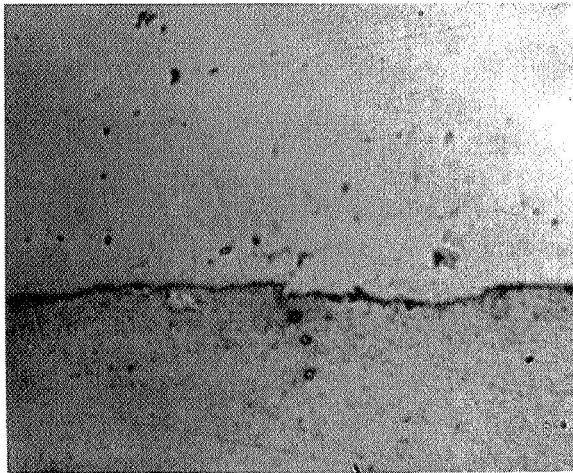0.5 in 347 SS Welded Tubing

Pit Type Specimen	I	II	III	IV	V
1	29	0	3	8	1
2	22	1	6	3	3
3	17	1	7	3	5
4	30	3	3	5	11
5	36	2	1	12	4
6	34	5	3	18	5
7	24	5	4	8	7
8	26	2	5	12	3
9	32	0	4	9	6
10	36	3	5	8	2
Total	286	22	41	81	47
Average	28.6	2.2	4.1	8.1	4.7

Number of Pits at O.D.
0.5 in SS347 Seamless Tubing

Pit Type/ Specimen No.	I	II	III	IV	V
11	14	1	1	4	7
12	14	3	3	8	3
13	7	0	1	3	2
14	6	1	3	5	1
15	7	0	1	3	1
16	9	1	2	4	1
17	9	1	1	4	0
18	6	3	7	5	0
19	6	0	4	4	0
20	6	1	2	0	2
Total	84	11	25	40	17
Average	8.4	1.1	2.5	4.0	1.7

MTI-10087

characteristics. This limited study rendered some support to various postulated mechanisms cited above in a qualitative manner, for instance Type II pits shown in Table II may be regarded as re-entrant pits, but it is not sufficiently precise to discriminate the various postulations with respect to their relative credence.

The alternative models led to qualitively similar formulas for the incipient boiling condition:

Holtz-Chen-Dwyer Model: [12,23,24]

$$\Delta P_{inc} = \frac{\sigma}{\sigma'} \; (P' - P_v') - \frac{G_o}{r_m^3} \; (T + \frac{\sigma}{\sigma'} T') \tag{2}$$

Re-entrant Cavity Model: [6]

$$\Delta P_{inc} = \frac{\sigma}{\alpha\sigma'} \; (P' - P_v') - \frac{P_g'}{T'} \; (T + \frac{\sigma}{\alpha\sigma'} T') \tag{3}$$

where primed quantities are those at the most severe deactivating condition, $G_o = P_{go} r_o^3/T_o$ is a measure of the content of the noncondensible gas and α^* allows the interface radius at inception of boiling to be different from that during deactivation. Geometrical parameters in the Holtz-Chen-Dwyer model are shown in Fig. 3. These two formulae predict similar trends in the effect of deactivation subcooling, the former correlates somewhat better with the experimental data. Incipient boiling superheats calculated according to the Holtz-Chen-Dwyer model for cesium and potassium are given in Figs. 4 through 9. In using these results, the following points should be borne in mind:

1. Because of the statistical nature of the phenomenon, the proposed prediction method would at best give an estimation of the most likely superheat. The actual superheat of any particular run may deviate from the predicted value by as much as $\pm$ 20°F since there was typically 40°F scatter in a most carefully controlled experiment.

2. G_o should be best regarded as an empirical constant established in recent experiments on deactivation history, instead of rigidly interpreted according to any particular model.

---

*Estimated to be about 1.5.

Initial Filling   Deactivation
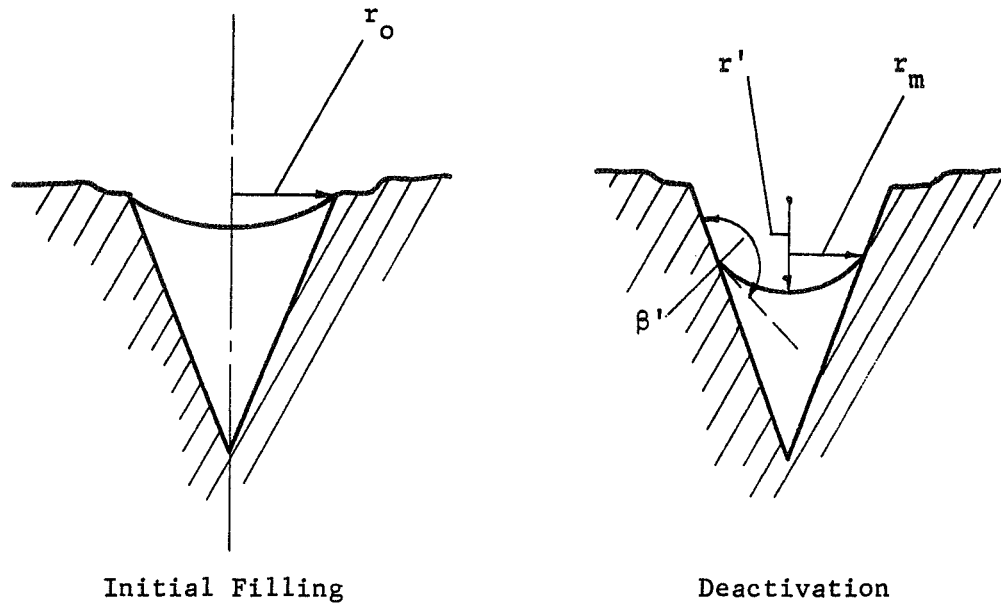
Fig. 3   Geometrical Parameters in the Holtz-Chen-Dwyer
          Model for Deactivation
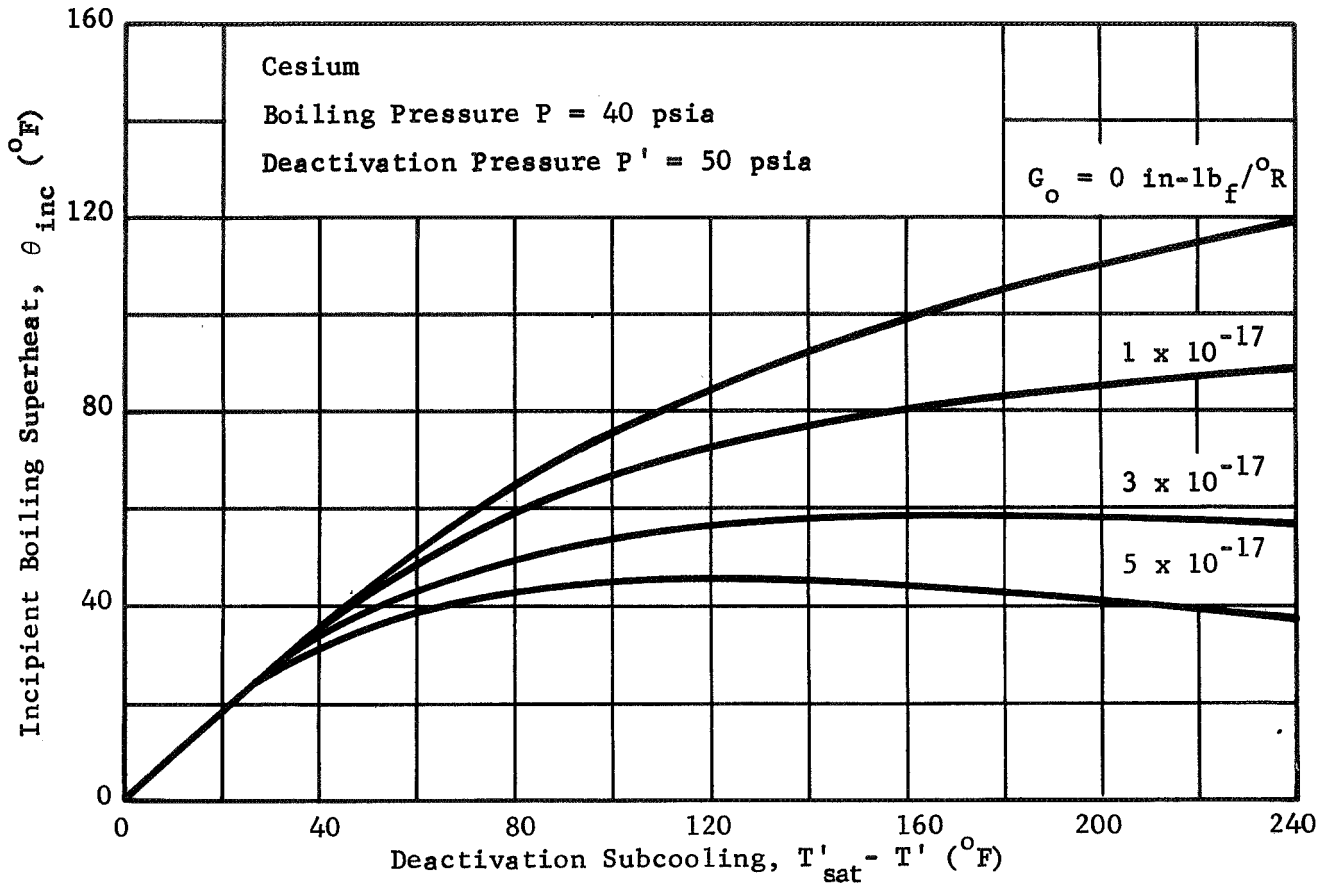
Fig. 4   Incipient Superheat vs Deactivation Subcooling for Cesium
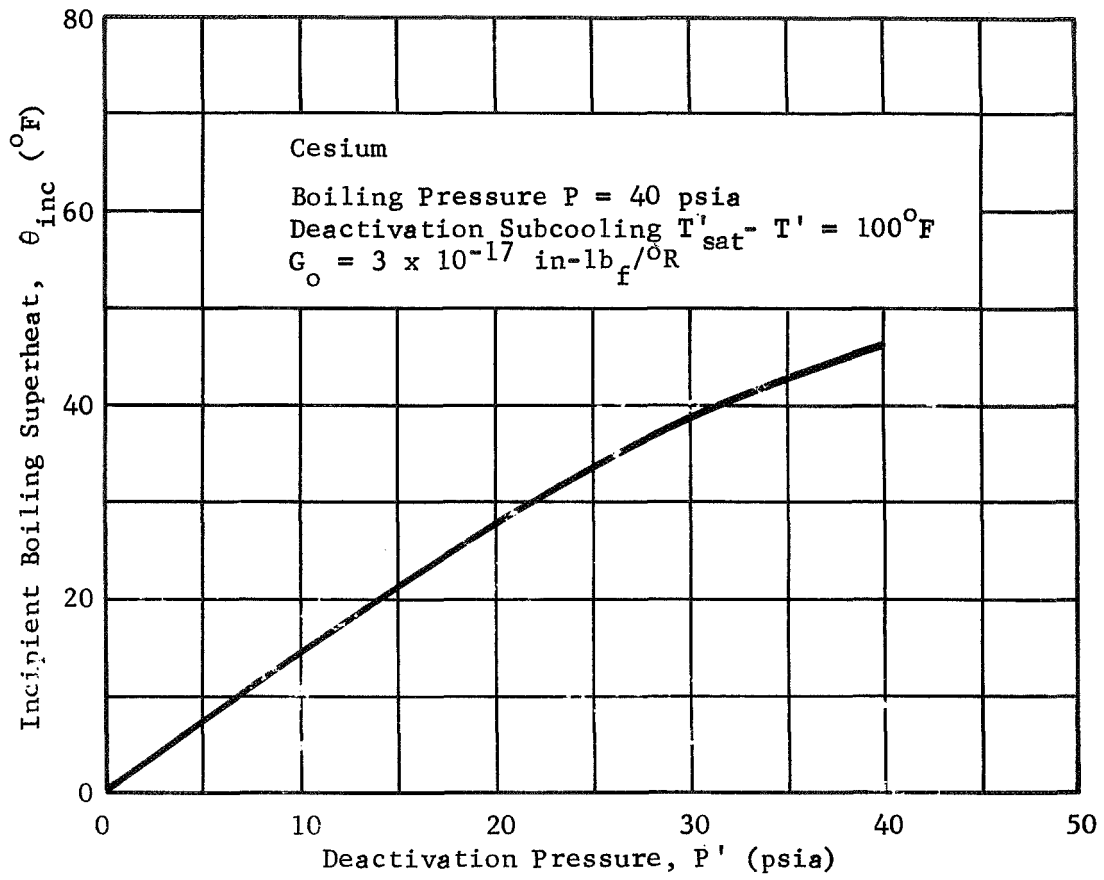
Fig. 5   Incipient Superheat vs Deactivation Pressure for Cesium
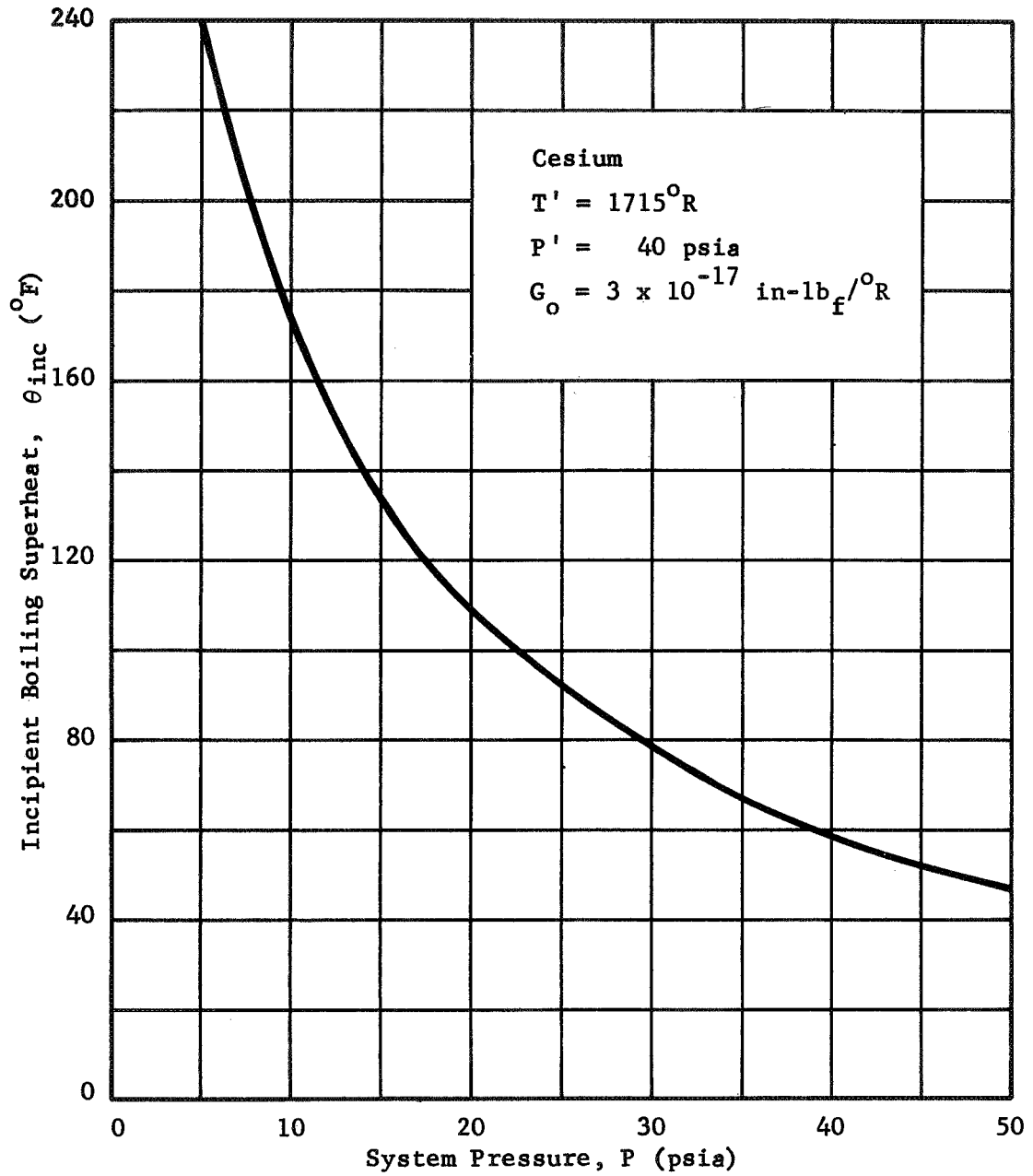
Fig. 6   Incipient Superheat vs System Pressure for Cesium
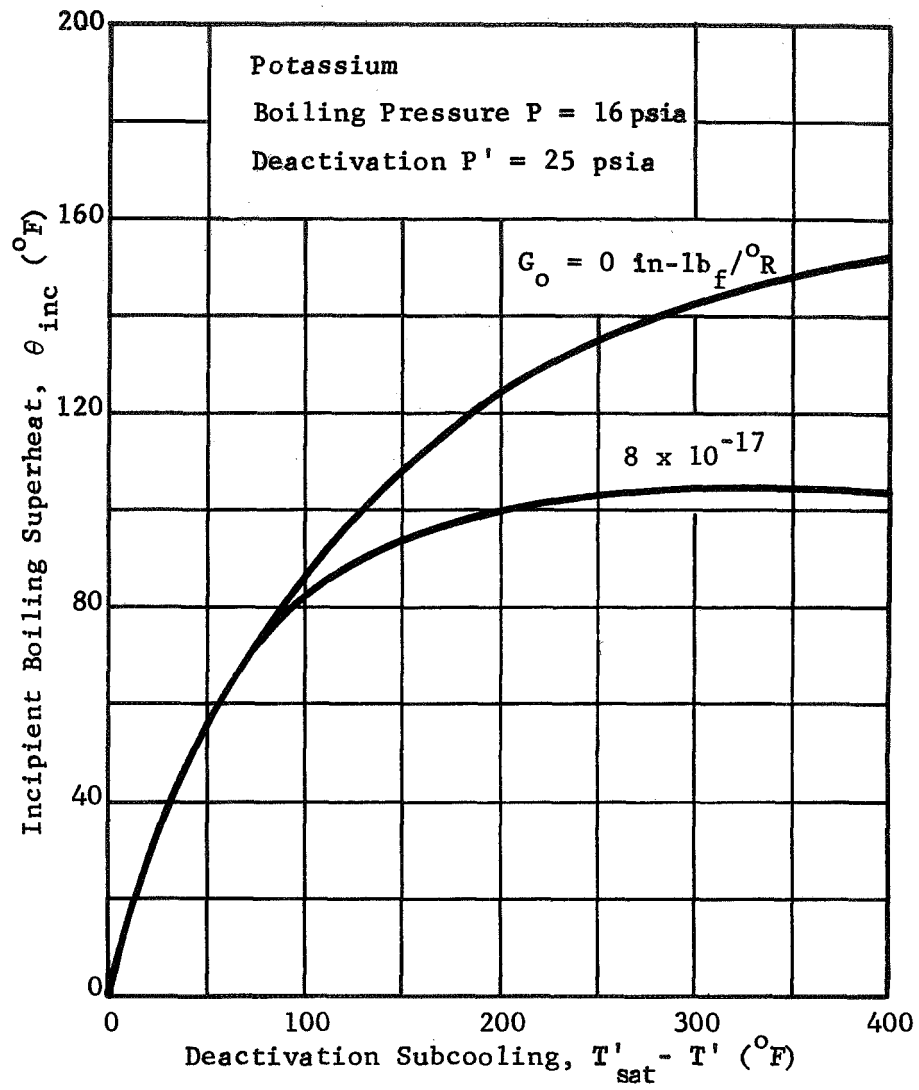
Fig. 7   Incipient Superheat vs Deactivation
Subcooling for Potassium
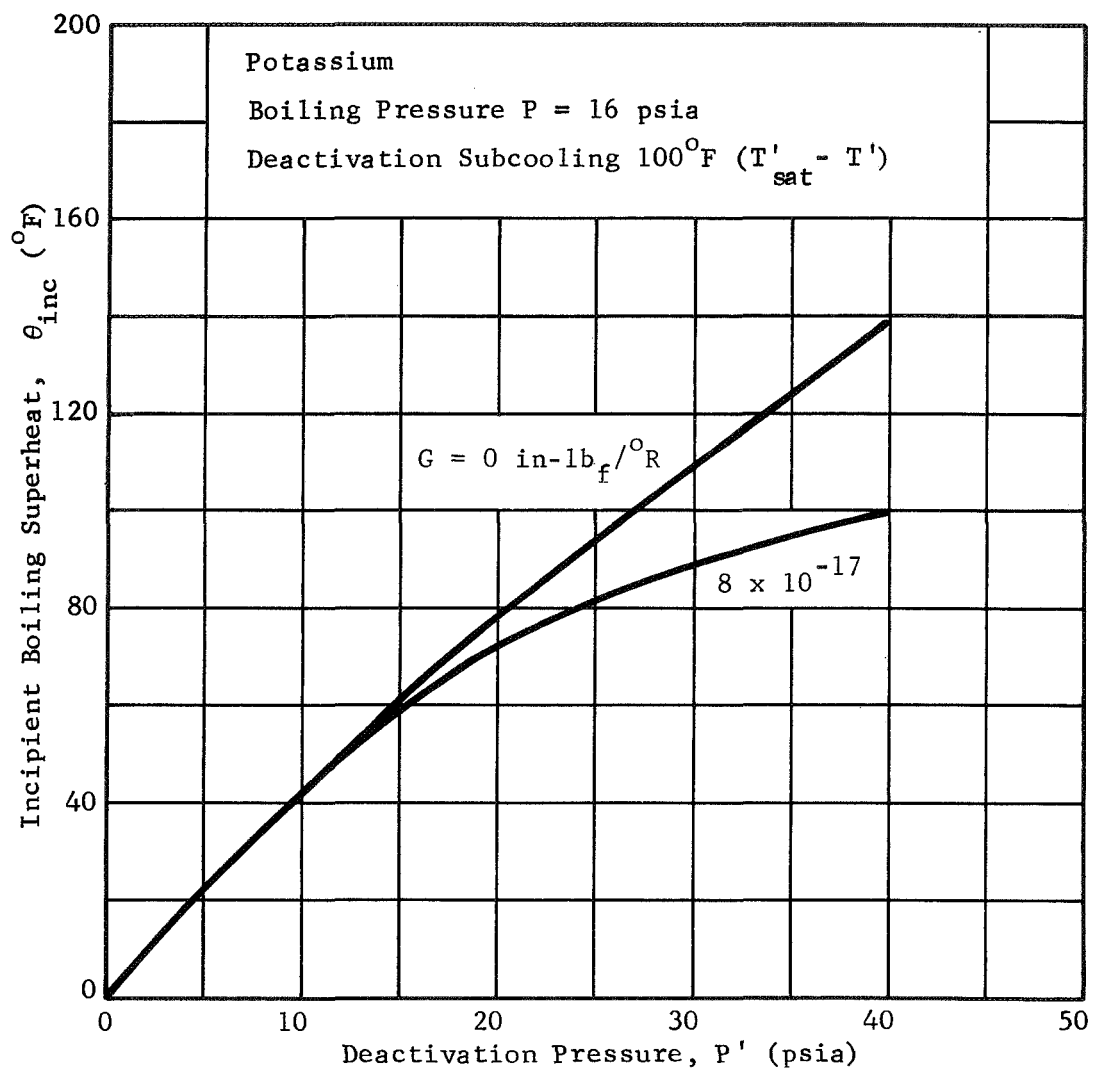
Fig. 8   Incipient Superheat vs Deactivation Pressure for
         Potassium
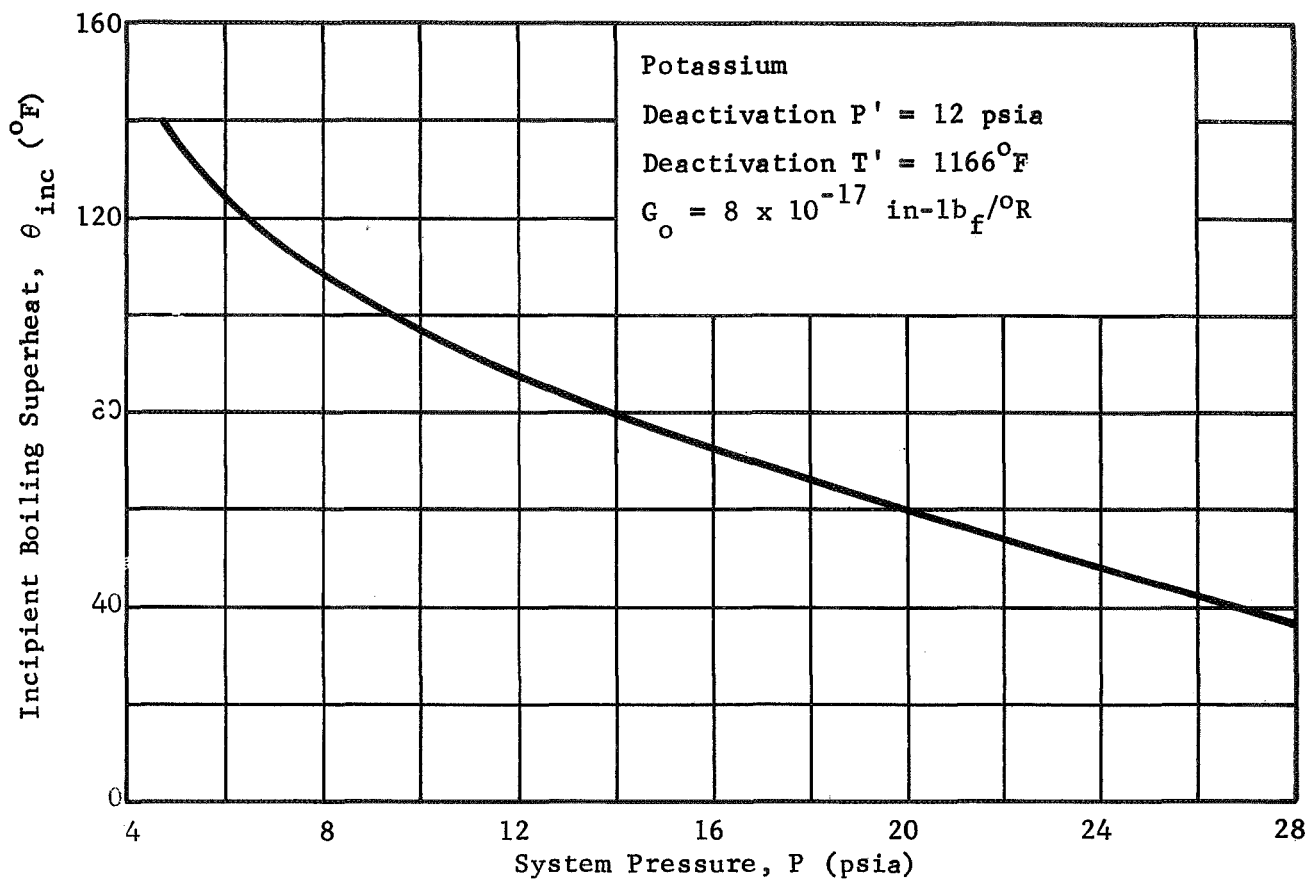
Fig. 9   Incipient Superheat vs System Pressure for Potassium

3. Data used in establishing the correlation were obtained with test appa-
   ratus built of commercial grade materials and would not be applicable
   to specially treated surfaces.

Other relevant factors recognized are heat flux and flow rate. Available data
are too scanty to warrant any definitive conclusions at this moment.

For "common" fluids with relatively poor thermal conductivity, substantial tem-
perature gradients can be present in the vicinity of the nucleation sites. It
has been postulated [25-28] that boiling incipience would commence only if the
fluid temperature at the bubble height is high enough to enhance bubble growth.
Thus, the required wall superheat would increase with heat flux as shown in Fig.
10 for water. This criterion does not by itself contradict the Holtz-Chen-Dwyer
criterion. In fact, for "common" fluids, both criteria should be checked, that
giving the higher superheat would dominate. For water due to the likelihood of
ample noncondensible gas in the nucleating cavities, the heat-flux criterion
is most likely to prevail.
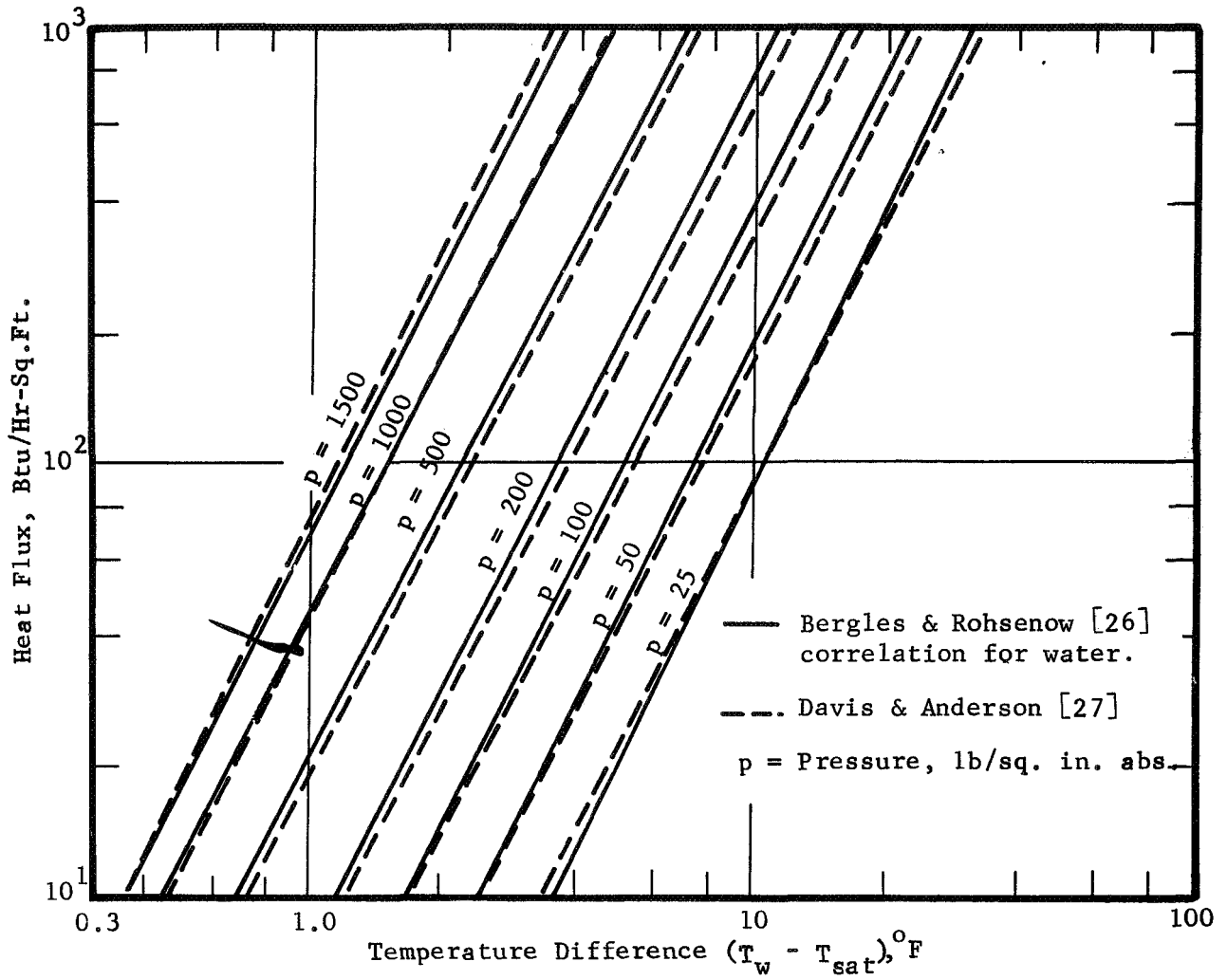
Fig. 10   Curves of Incipient Boiling Superheat vs Heat Flux for Water

VOID GROWTH AND EVAPORATION RATE

When boiling occurs in a superheated liquid, vapor generation is accompanied
by substantial pressure rise which in turn induces hydrodynamic disturbances.
The degree of violence of the latter would largely depend on the vapor generation
rate.

In the second topical report [29], two different modes of vapor generation in the
initial stage have been considered. The first one dealt with the growth of a
small bubble, presumably coming from a wall nucleation site, in the superheated
liquid. Such bubbles, while increasing in its size, would be swept downstream.
If the liquid flow speed is low in comparison with the bubble growth rate, then
the very first bubble to appear would quickly fill up the duct cross-section in
the form of a large void. Subsequent vaporization would then appear as the prop-
agation of the void upstream, with phase change occuring across the head of the
void while the presence of any other bubbles or the lack of it would play a rath-
er insignificant role. The latter situation is most likely to take place in
liquid metal boiling and was separately studied as the second mode of void growth.
Analyses of these two problems are summarized under the section heading "Void
Growth Mechanizms".

In addition to these two "early stage" evaporation modes there are two other im-
portant modes in forced convective boiling; they are the annular and the dispersed
flow regimes. Thermodynamic equilibrium is approximately maintained in the annu-
lar flow regime, while evaporation in the dispersed flow regime again become
characterized by superheating not only of the liquid phase, but also of the duct
wall and of the vapor phase. Under thermodynamic non-equilibrium, the evaporation
rate is essentially controlled by simultaneous mass and heat transports. This
view was stressed in the derivation of the evaporation rates in [29] , the results
of which are collected under the heading "Constitutive Equations for Evaporative
Processes".

VOID GROWTH MECHANISMS

Growth Rate of Vapor Bubble

The growth of a vapor bubble in a superheated liquid subsequent to incipient nucleation is governed by the simultaneous actions of several physical processes; namely

    (1)   heat conduction in the liquid with the vaporization occurring at the interface behaving as a heat sink,

    (2)   inertia of the liquid being displaced by the growing vapor bubble,

    (3)   mass transfer kinetics at the interface, and

    (4)   surface tension of the liquid

Historically, various aspects of this problem were considered by numerous investigators [30, 31, 32, 33, 34, 35, 36, 37, 38, 39]. From the standpoint of a generally applicable analysis, all above cited processes should be considered. Satisfactory formulations of such an analysis already exist [37, 38, 39], however, the required computations to obtain results for a large number of fluids and environmental conditions turned out to be rather tedious; consequently only a limited amount of usable numerical information has been published. Thus, a major objective with respect to this topic is to establish a generally applicable but also convenient computation procedure for the bubble growth rate. This objective was made possible by invoking a number of simplifying assumptions which can be subsequently verified a posteriori with the calculated results. The major assumptions so invoked include

    (1)   The vapor bubble is quasi-quiescent. The change (increase) in its mass content due to density change is negligible in comparison with that due to its size change (growth).

(2) Expansion work done by the growing bubble is approximated by a constant pressure process.

(3) Temperature profile in the thermal boundary layer around the bubble is parabolic.

(4) Energy transfer across the bubble boundary is dominated by the balance between heat conduction through the liquid and the latent heat of evaporation.

(5) The thermal boundary layer thickness is small in comparison with the bubble radius.

(6) Mass transfer kinetics at the interface takes place isothermally approximately at the liquid ambient temperature.

(7) The Clausius-Clapeyron relation is approximated by a straight line in the T-P diagram joining the saturation states corresponding to the liquid ambient temperature and pressure.

Consequently, six equations are derived in [29] which were given as Eqs. (11), (17), (23), (26), (27) and (34) there:

$$\dot{R}_v = \sqrt{\frac{2g_c}{3\rho_L} \left[(P_v - P_\infty)(1 - \frac{R_o^3}{R_v^3}) - \frac{3\sigma}{R_v}(1 - \frac{R_o^2}{R_v^2}) \right]} \tag{4}$$

$$2K_L \left(\frac{T_\infty - T_L}{R_L - R_v} \right) = h_{fg} \, \rho_v \, \dot{R}_v \tag{5}$$

$$C_p \rho_L (T_\infty - T_L)(R_L - R_v) = h_{fg} \, \rho_v \, R_v (1 - \frac{R_o^3}{R_v^3}) \tag{6}$$

$$\dot{R}_v = \frac{C}{\rho_v} \sqrt{\frac{g_c}{2\pi R T_\infty}} (P_L^* - P_v) \tag{7}$$

$$P_{L\infty}^{*} - P_{L}^{*} = \quad (T_{\infty} - T_{L}) \tag{8}$$

$$\rho_{v} = \frac{P_{v}}{RT_{sat}} \tag{9}$$

which simultaneously determine the six unknowns: $\dot{R}_{v}$, P_{v}, T_{L}, P_{L}^{*}, $(R_{L} - R_{v})$, and ρ_{v}. The symbols in these equations represent

C	=	coefficient of evaporation (and condensation)
g_{c}	=	gravitational constant
h_{fg}	=	latent heat of vaporization
K_{L}	=	thermal conductivity of liquid
P_{L}^{*}	=	saturation pressure corresponding to T_{L}
$P_{L\infty}^{*}$	=	saturation temperature at T_{∞}
P_{v}	=	pressure of vapor (inside bubble)
P_{∞}	=	ambient liquid pressure
R	=	gas constant of vapor
R_{L}	=	radius at edge of thermal boundary layer
R_{o}	=	initial radius of bubble
R_{v}	=	radius of vapor bubble
$\dot{R}_{v}$	=	time rate of growth of bubble radius
T_{L}	=	liquid temperature at interface
T_{sat}	=	saturation temperature at P_{∞}
T_{∞}	=	ambient liquid temperature
κ	=	$\dfrac{dP}{dT}\bigg|_{sat}$ = constant in the linear approximation of the Clausius-Clapeyron relation
ρ_{L}	=	liquid density
ρ_{v}	=	vapor density inside bubble
σ	=	surface tension of liquid (at P_{∞} and T_{sat})

Numerically computed results from above equations are compared with the more precise ones given in [37] respectively for sodium at 14.7 psia with a superheat of 273°F and for water at 1.47 psia with a superheat of 4.81°F in Figs. 11 and 12. It is seen that the error of the present approximate analysis is at its worse for water at low pressure, but even then is no more than 16%. Further more, it is seen that for the wide range of bubble size, e.g. $10 < R_v/R_o < 10^4$ for sodium, $\dot{R}_v$ is practically constant, approximately equal to its maximum for each value of C. Consequently, it is useful to present the maximum $\dot{R}_v$ (for each C). This is done in Figs. 13, 14 and 15 respectively for water, potassium, and cesium, in which the maximum bubble growth rate at atmospheric pressure is plotted against superheat for three values of the vaporization coefficient.

In Fig. 16, the maximum bubble growth rate is plotted against system pressure at a constant superheat for potassium, again for three values of the vaporization coefficient. For a large vaporization coefficient, e.g. C = 1, bubble growth is controlled by inertia, then an increase in system pressure primarily results in an increase in the driving force $\kappa = \dfrac{dP}{dT}\Big|_{sat}$; therefore, the maximum bubble growth rate increases monotonically with the system pressure. On the other hand, for a small vaporization coefficient, e.g. C = 0.01, the bubble growth rate tends to be limited by mass transfer, and since the vapor density would increase with system pressure, the maximum bubble growth rate tends to decrease with the system pressure instead.

Assuming the vaporization coefficient is fairly large, e.g. C = 1, then, from the numerical results in Figs. 13, 14 and 15, the maximum bubble growth rate is in excess of 10^2 cm/sec. This is especially true in the case of the two alkali metals considered. Thus, for typical convective boiling situations, the bubble growth rate is likely to be much larger than the convective velocity. Then once incipient nucleation has started, the rapidly growing bubbles would quickly fill up most of the flow passage cross section to cause the flow to change from the all liquid situation into the annular flow regime. For this reason, one may neglect altogether the bubble flow regime, and with sufficient superheat, vaporization would take place in the form of a propagation of the head of the annular flow regime upstream of the point of inception of nucleation.
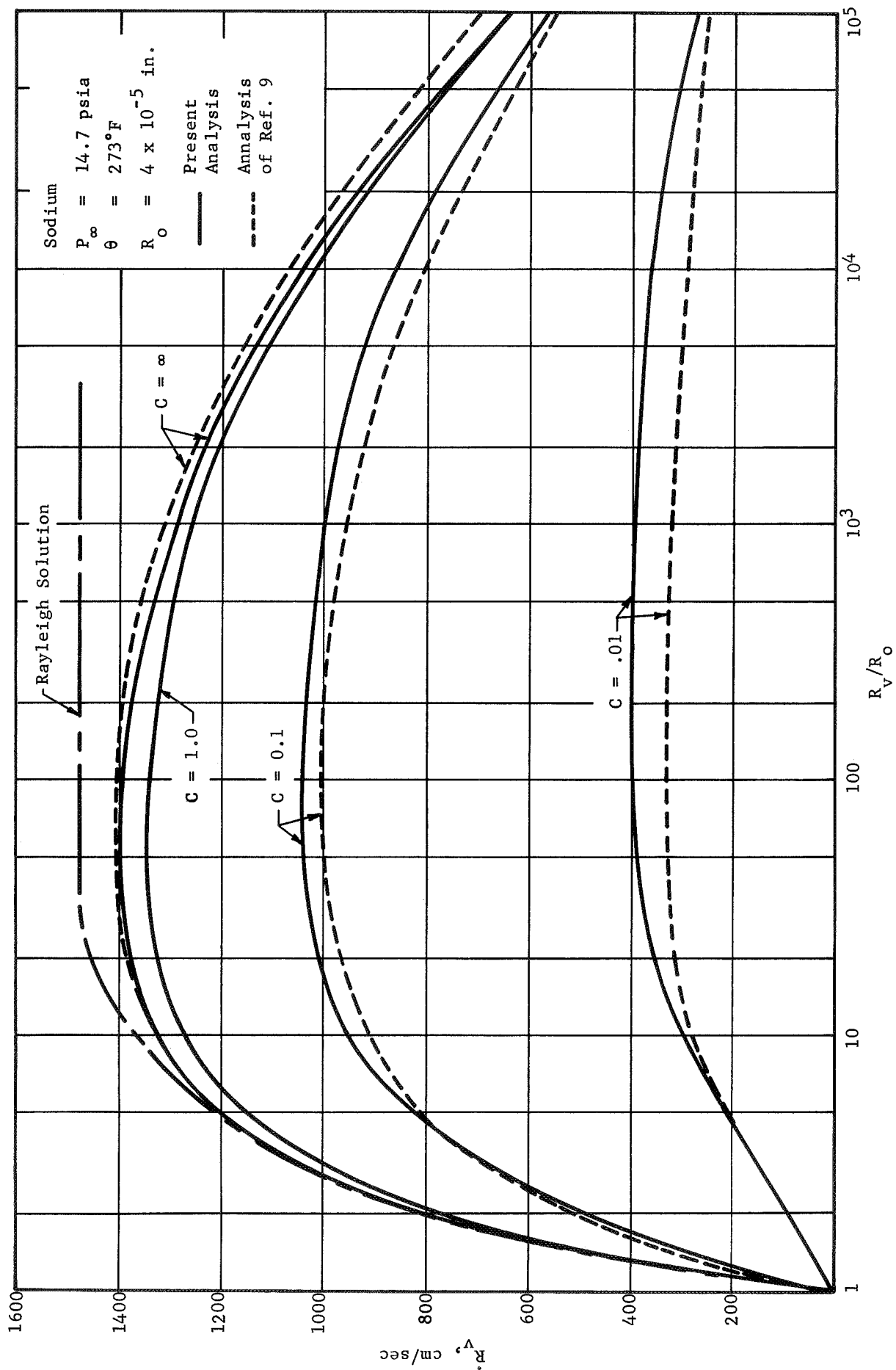
Fig. 11   Bubble Growth Rate for Superheated Sodium

26
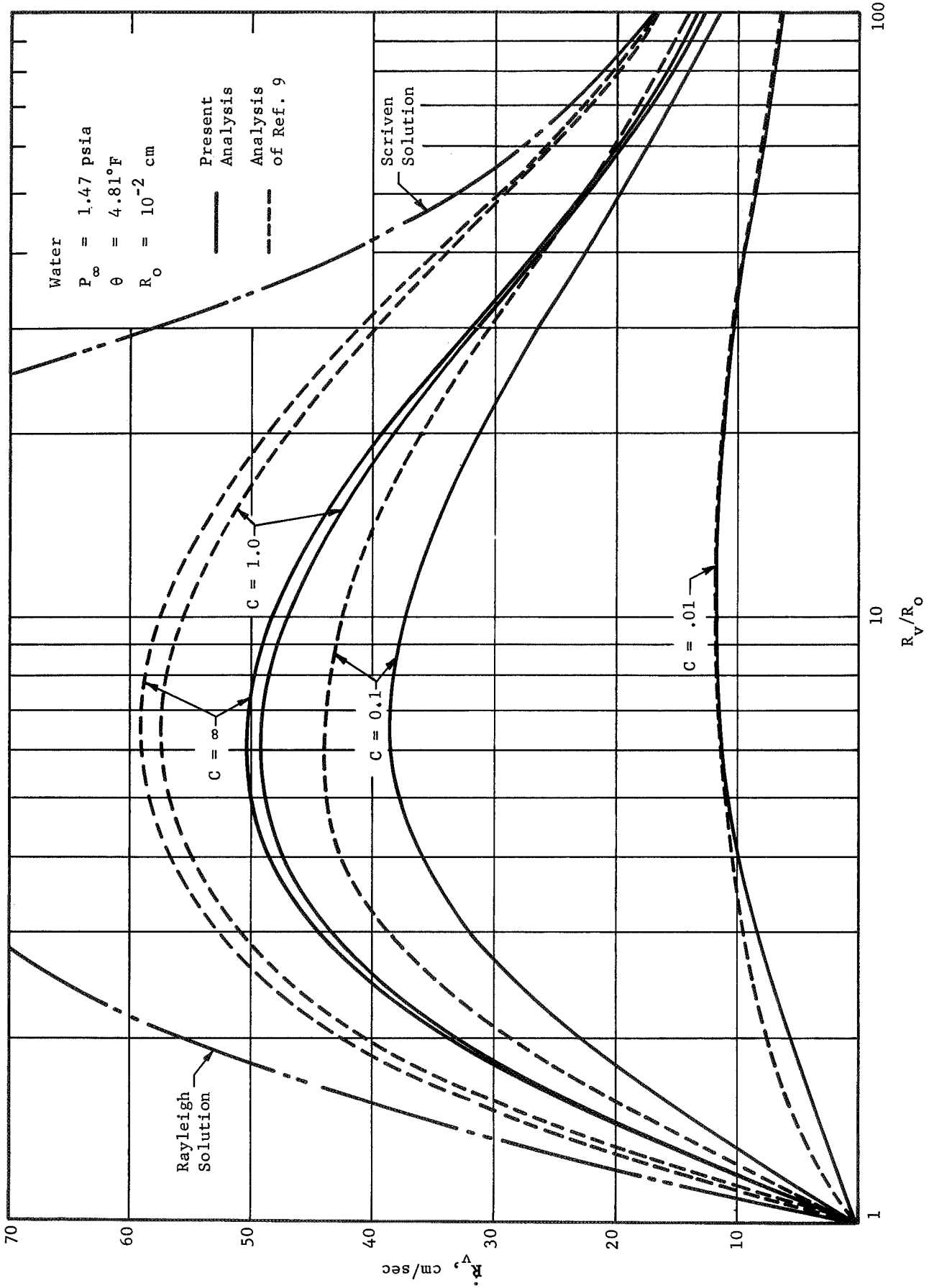
Fig. 12   Bubble Growth Rate for Superheated Water

MTI-10074

$P_\infty = 14.7$ psia

900

800

700

$C = 1.0$

600

$C = 0.1$

500

$\dot{R}_v$, cm/sec

400

300

200

$C = .01$

100

10   20   30   40   50   60

θ
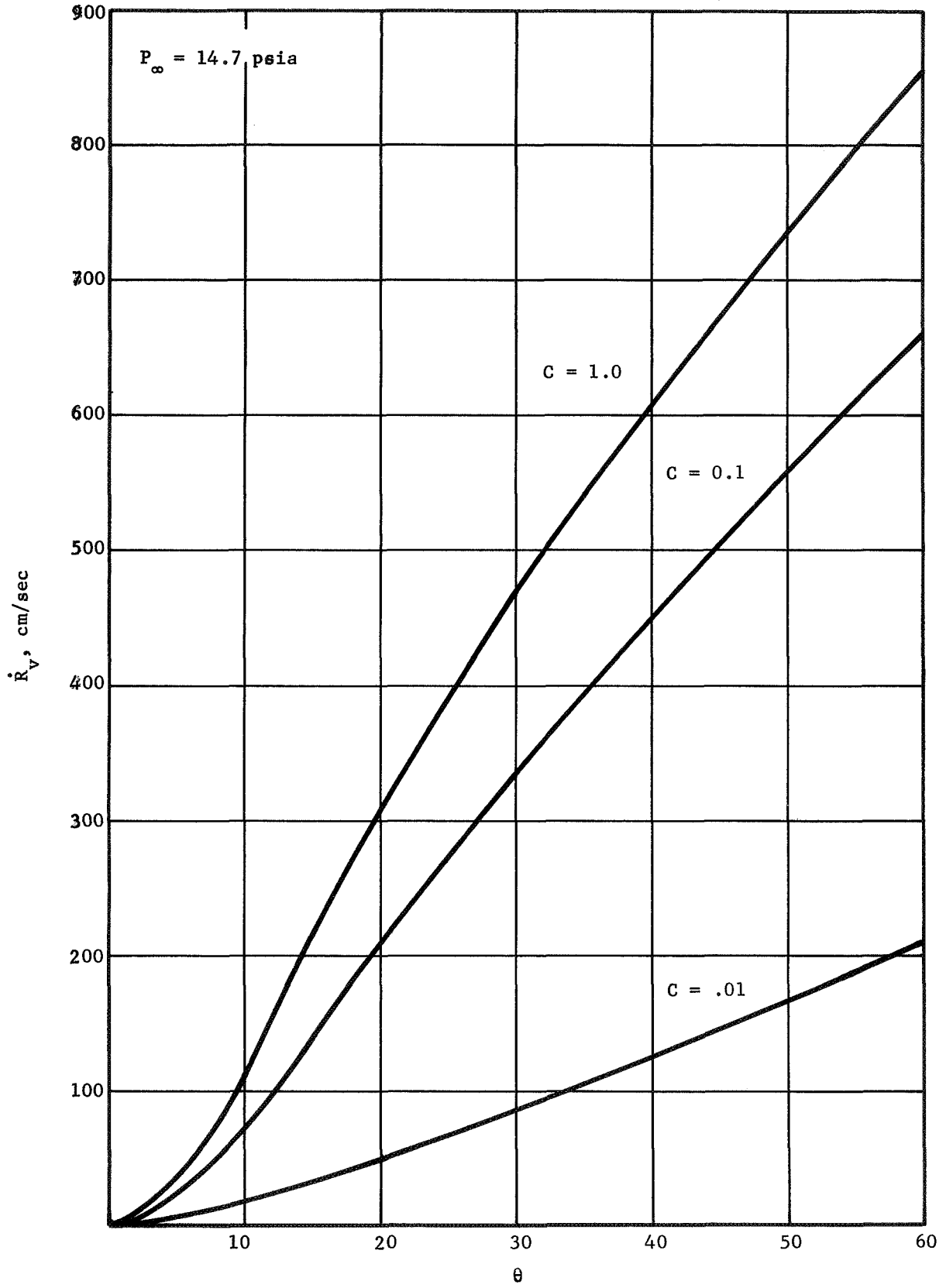
Fig. 13   Bubble Growth Rate vs Superheat in Water
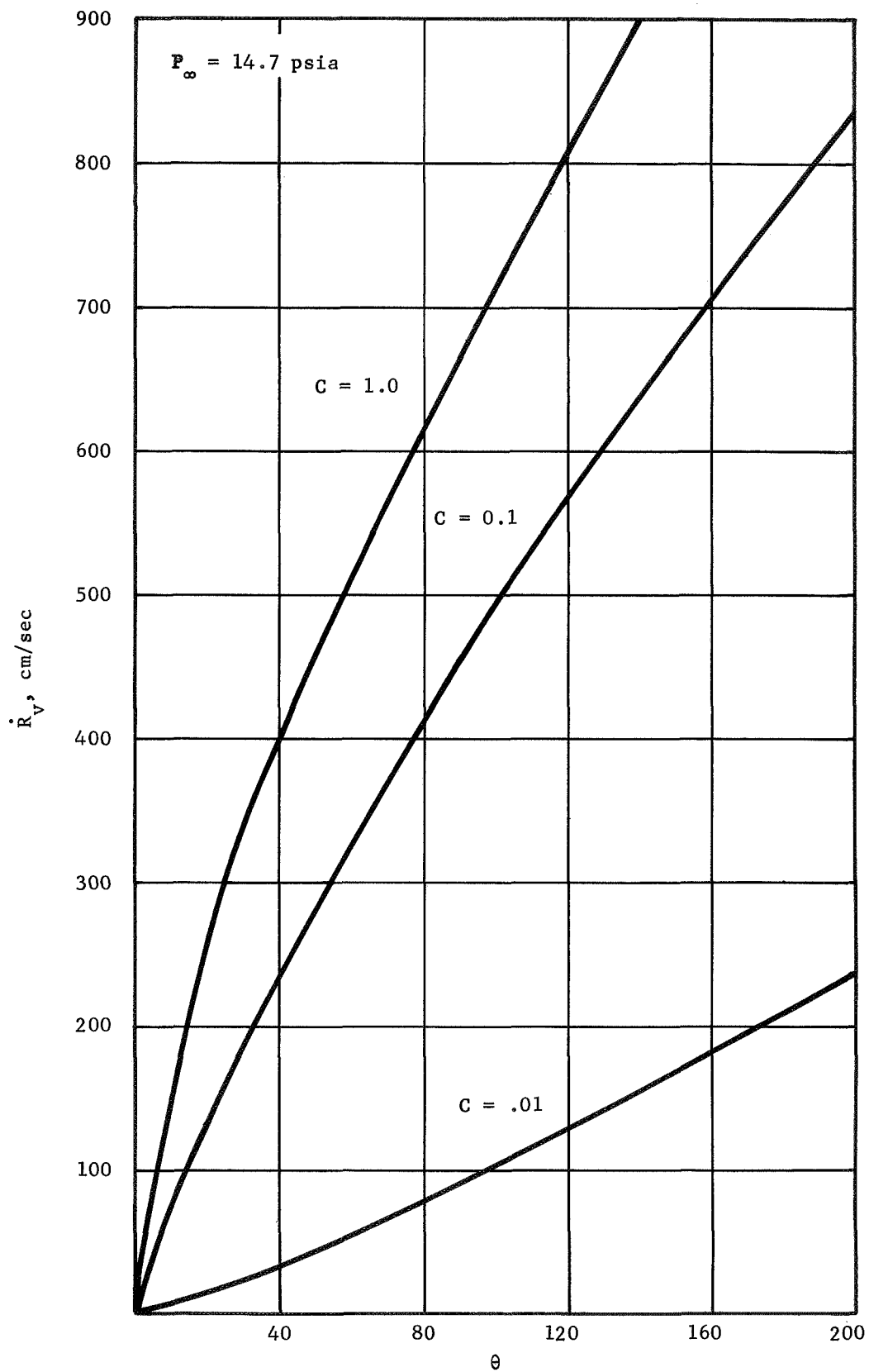
Fig. 14   Maximum Bubble Growth Rate vs Superheat in Potassium
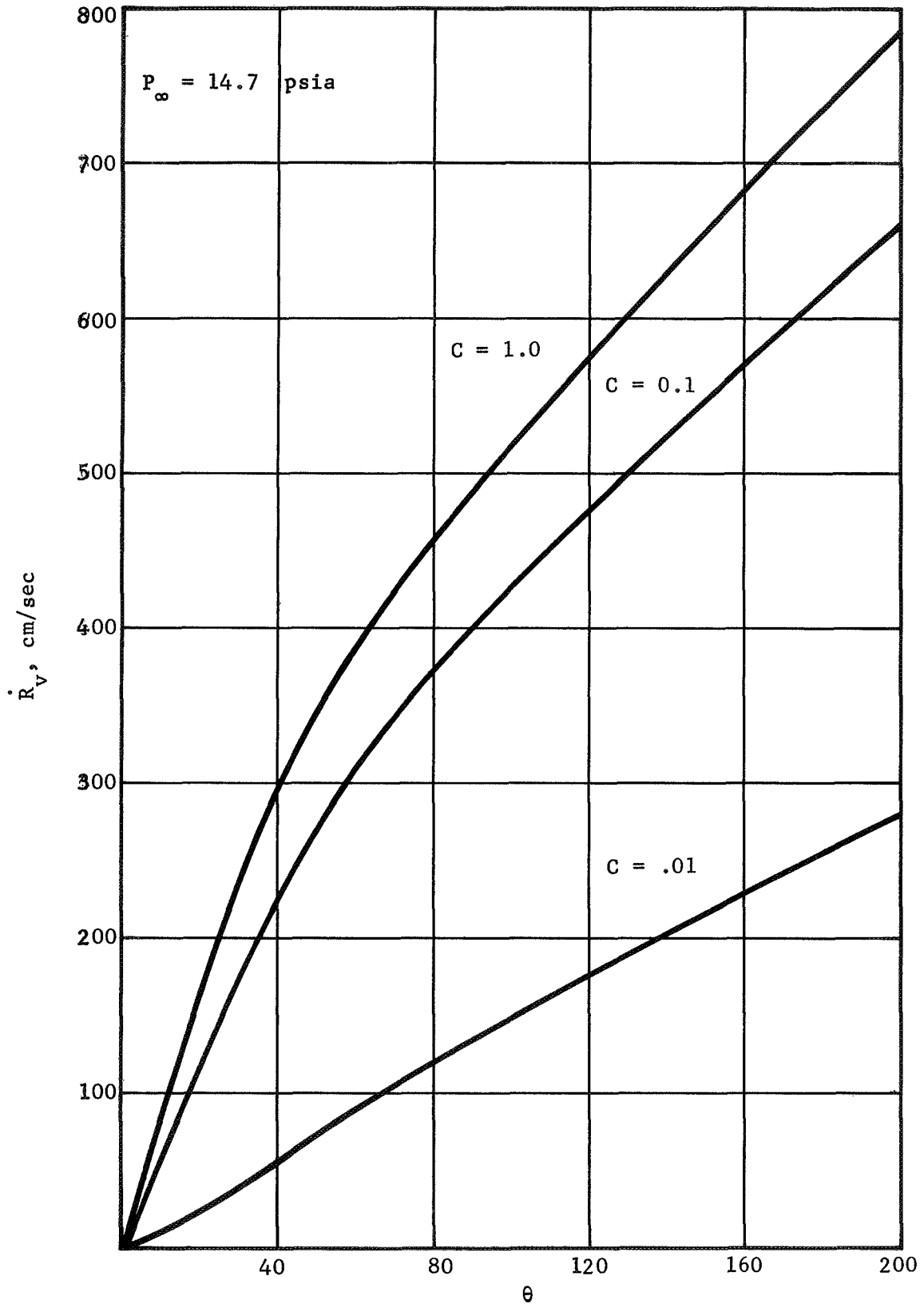
Fig. 15   Maximum Bubble Growth Rate vs Superheat in Cesium
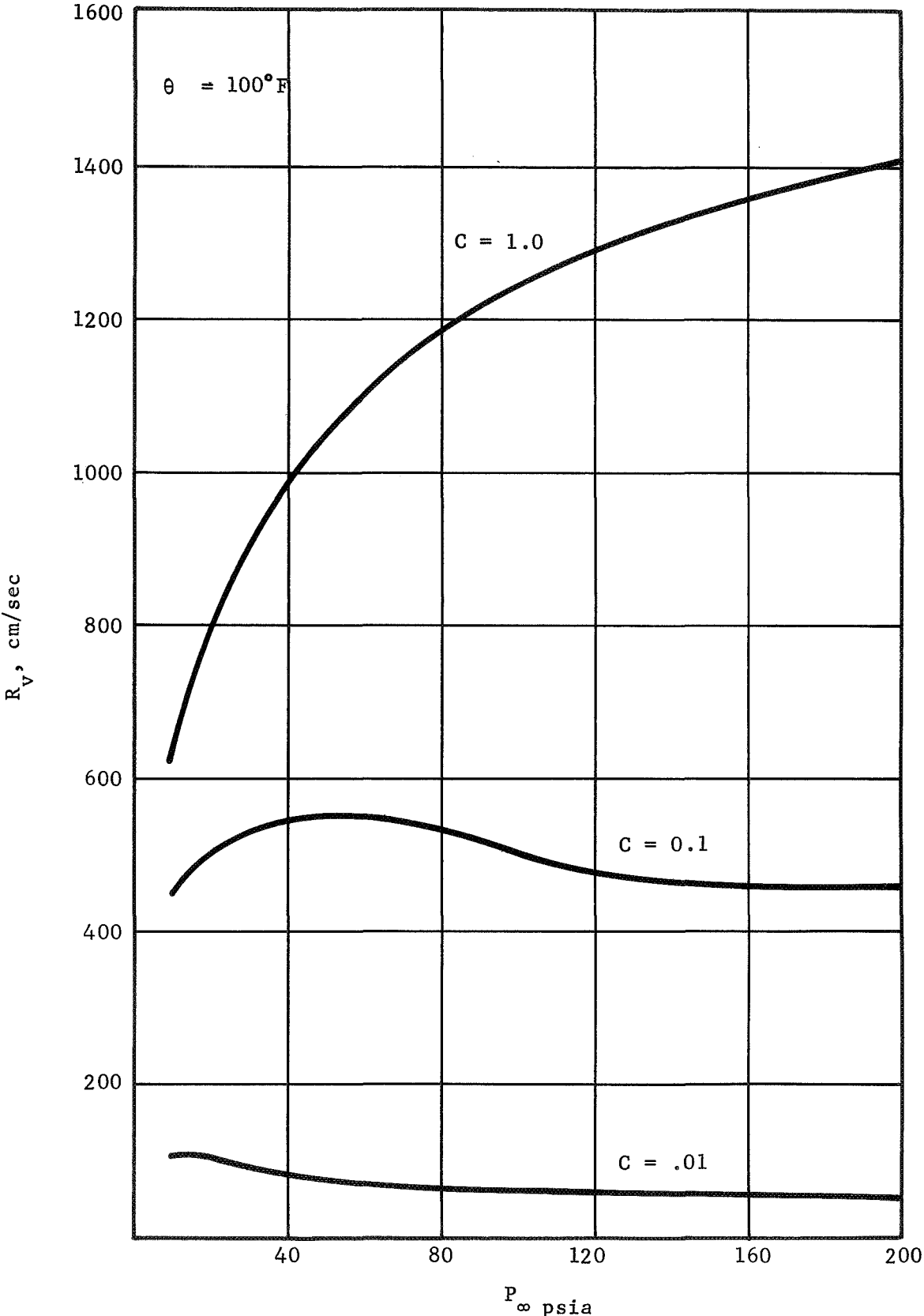
Fig. 16   Maximum Bubble Growth Rate vs System Pressure in Potassium

Propagation of Vapor Void

During non-equilibrium boiling, once incipient nucleation has started, void propagation is likely to extend into regions where wall nucleation sites are not available due to a large bubble growth rate. It is useful to consider an analysis of such a mechanism. In [29], the problem of void propagation in a constant head duct was formulated. The considered situation is illustrated schematically in Fig. 17. The principal assumptions employed in this formulation consist of:

(1) The liquid in the duct is initially superheated (at least at the exit).

(2) The heat input per unit length of duct is maintained constant.

(3) The head drop across the length of the duct is balanced by the sum of the friction loss in the liquid section, inertia of the liquid column, pressure drop across the head of the void, and friction loss in the annular flow section.

(4) A constant friction factor is used to calculate friction losses in either the liquid flow and the annular flow regions.

(5) Duct cross-section is constant and flow velocity in the liquid column is uniform at all instants.

(6) The linearized Clausius-Clapeyron relation based on the inlet temperature is used.

(7) Levy's "momentum exchange model" [49], is extended to yield a relation between the void fraction and the flow quality.

(8) Pressure of vapor at the head of the void is in equilibrium with the stagnation pressure of the liquid relative to the propagating void and is equal to the saturation vapor pressure at the corresponding liquid temperature.
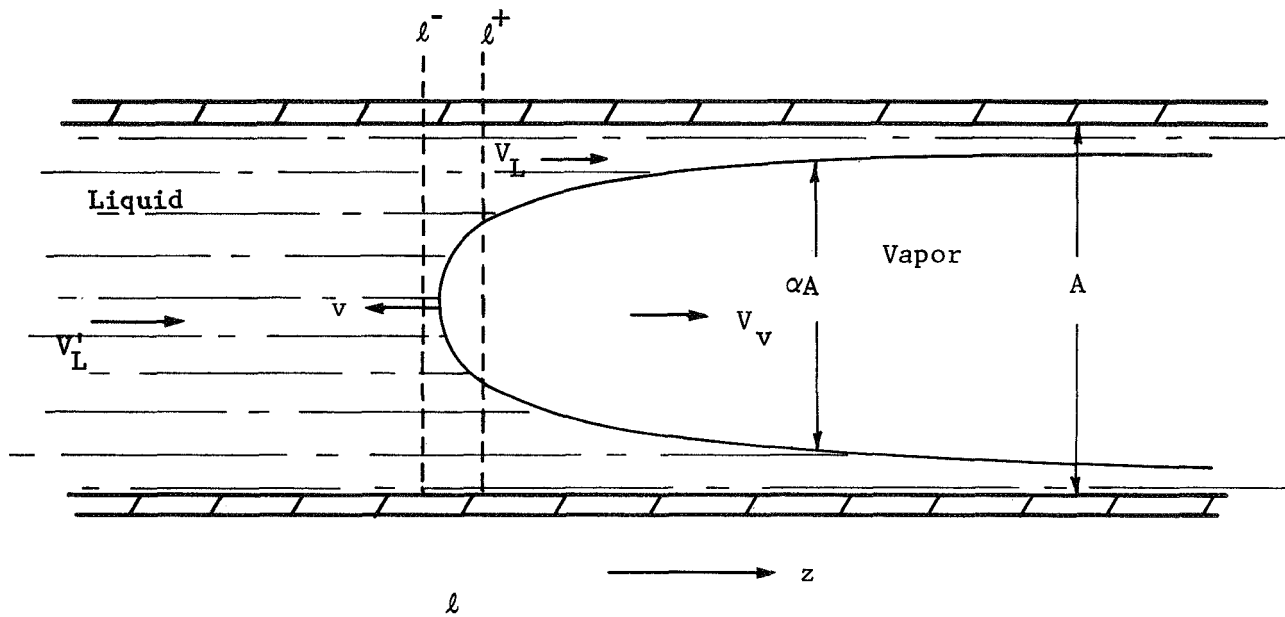
Fig. 17 Schematic of Propogating Void in Duct

The resulting governing equations are

$$\Delta P'(\ell < z \leq L) \;=\; \int_{\ell^+}^{z} \frac{f\rho_L}{g_c D}\left[(V_L' + v)\left(\frac{1-X'}{1-\alpha}\right) - v\right]^2 dz$$

$$+ \;\rho_L \frac{(V_L' + v)^2}{g_c}\left[\frac{(1-X')^2}{1-\alpha} - \frac{(1-X_\ell')^2}{1-\alpha_\ell} + \frac{\rho_L}{\rho_v}\left(\frac{X'^2}{\alpha} - \frac{X_\ell'^2}{\alpha_\ell}\right)\right] \tag{10}$$

$$\overline{\Delta P} \;=\; H - \Delta P_L' \tag{11}$$

$$\theta \;=\; \frac{q\ell}{\rho_L V_L' A (C_P)_L^+} \;+\; \theta_{in} + \left(\frac{dT}{dp}\right)_{sat}\overline{\Delta P} \tag{12}$$

$$X'(\ell < z \leq L) \;=\; \frac{q(z-\ell)}{\rho_L(V_L'+v)A\,h_{fg}} \;+\; \frac{(C_P)_L}{h_{fg}}\left[\theta + \left(\frac{dT}{dp}\right)_{sat}\Delta P'\right] \tag{13}$$

$$X' \;=\; \alpha\left\{\frac{(1-2\alpha) + \sqrt{(1-2\alpha)^2 + \alpha[2\frac{\rho_L}{\rho_v}(1-\alpha)^2 + \alpha(1-2\alpha)]}}{2\left(\frac{\rho_L}{\rho_v}\right)(1-\alpha)^2 + \alpha(1-2\alpha)}\right\} \tag{14}$$

$$V_L' + v \;=\; \left(\frac{1-\alpha_\ell}{1-X_\ell'}\right)\sqrt{\frac{2g_c}{\rho_L}\frac{\theta}{(dT/dp)_{sat}}} \tag{15}$$

$$\Delta P \;=\; \rho_L\frac{(V_L' + v)^2}{2g_c}\left[\left(\frac{1-X_\ell'}{1-\alpha_\ell}\right)^2 - 1\right] \tag{16}$$

$$\dot{V}_L' \;=\; \frac{g_c}{\rho_L \ell}(\overline{\Delta P} - \Delta P) - \frac{fV_L'^2}{D} \tag{17}$$

A	=	cross-sectional area of duct
$(C_P)_L$	=	specific heat at constant pressure of liquid
D	=	hydraulic diameter of duct
$(dT/dp)_{sat}$	=	Clausius-Clapeyron line
f	=	friction factor
g_c	=	gravitational constant
H	=	total head maintained across the duct
L	=	length of duct
ℓ	=	location of the head of the void
ℓ^+	=	location immediately downstream of the head of the void
q	=	heat flux per unit length of duct
V_L'	=	flow velocity of liquid
$\dot{V}_L$	=	time derivative of the flow velocity of the liquid column
v	=	void propagation speed (positive upstreams)
X'	=	vapor mass flow quality relative to the head of the void
α	=	area fraction of vapor
h_{fg}	=	specific latent enthalpy for evaporation
ΔP	=	pressure drop across the head of the void
$\Delta \bar{P}$	=	pressure drop from inlet to ℓ^+
$\Delta P'$	=	pressure drop in the annular flow region from the head of the void
θ	=	superheat at ℓ^+
θ_{in}	=	superheat at inlet (may be negative)
ρ_L	=	liquid density
ρ_v	=	vapor density
$(\ )_\ell$	=	$(\ )$ at $(z=\ell)$

The above set of equations appeared in [29] as Eqs. (41), (42), (52), (59), (63), (64), (69); the order of their appearance have been altered and some minor rearrangements have been made for clarity of presentation.

In the first approximation, $(dT/dp)_{sat}$, ρ_v, h_{fg}, and f may be regarded as system invariants. Clearly, accuracy of the analysis would be improved by evaluating them in accordance with the local thermodynamic and hydrodynamic considerations. L, D, A, ρ_L, g_c, and H are clearly all constants. Given V_L', Eqs. (10) through (16) can be solved simultaneously for ($\Delta P'$, $\Delta \bar{P}$, θ, X', α, $V_L' + v$, and ΔP). Because of the nonlinear nature of these equations, a numerical method would be necessary. Subsequently, Eq. (17) can be integrated to obtain V_L' at a later instant; then the process can be repeated. In this manner, the nonequilibrium propagation of a void can be readily calculated.

CONSTITUTIVE EQUATIONS FOR EVAPORATIVE PROCESSES

In a forced convection evaporative flow, regardless of its specific flow structure, the concept of "source" of the vapor phase can be used to describe the rate of phase changes. Consider a duct of constant cross-sectional area A. At any given instant and location (t,z), the fraction of A through which the vapor phase flows is designated as αA, then the liquid phase flows through $(1-\alpha)A$. Thus the differential continuity condition is

$$\frac{\partial}{\partial t} [\alpha \rho_V + (1-\alpha) \rho_L] + \frac{\partial}{\partial z} [\alpha \rho_V V_V + (1-\alpha) \rho_L V_L] = 0 \tag{18}$$

which accounts for the total mass conservation of both liquid and vapor phases. ρ_V, ρ_L, V_V, V_L are respectively the densities and velocities of the vapor and liquid phases. The rate of generation of the vapor phase is [29]

$$\Gamma_V = \frac{\partial}{\partial t} (\alpha \rho_V) + \frac{\partial}{\partial z} (\alpha \rho_V V_V) \tag{19}$$

(A slightly different definition of vaporization rate was used in [40], where, $\bar{V} = [\alpha \rho_V V_V + (1-\alpha) \rho_L V_L]/[\alpha \rho_V + (1-\alpha) \rho_L]$ took the place of V_V in the above equation).

The corresponding latent heat must be derived from the heat addition to the duct and reduction in the sensible heat. Thus

$$\Gamma_V = \frac{1}{h_{fg}} \left\{ \frac{q}{A} + \frac{1}{J} \frac{\partial P}{\partial t} - (1-\alpha) \rho_L \left(\frac{\partial}{\partial t} + V_L \frac{\partial}{\partial z}\right) h_L - \alpha \rho_V \left(\frac{\partial}{\partial t} + V_V \frac{\partial}{\partial z}\right) h_V \right\} \tag{20}$$

h_{fg} is the specific latent enthalpy, q is the heat input per unit duct length, P is the pressure, h_L and h_V are the specific enthalpies of the respective phases. A complete analytical description of any forced convection evaporative flow must

in some way account for some knowledge of Γ_v as well as the slip-velocity $(V_v - V_L)$.

In the special case that thermodynamic equilibrium is approximately maintained, at each (t,z) the two phases would have the same temperature which is determined from $P(t,z)$ according to the equilibrium saturation state. That is,

$$dh_L = \left.\frac{dh_L}{dP}\right|_{sat} dP, \quad dh_v = \left.\frac{dh_v}{dP}\right|_{sat} dP \tag{21}$$

In general, both Γ_v and $(V_v - V_L)$ would depend on the flow structure or flow regime. Classification of two-phase flow structure recognizes the following flow regimes [41]:

(a) bubble flow

(b) coalescing flow

(c) annular flow

(d) dispersed flow

These flow regimes were established in forced convection experiments of air-water mixtures. In a boiling flow, particularly in the presence of superheat, transition from bubble flow to annular flow takes place very rapidly (see previous estimate on bubble growth rate) so that separate allowance for the presence of coalescing flow would not be necessary. In fact, with sufficient superheat, once boiling nucleation had commenced, bubbles would rapidly grow into a central void, which would then propagate upstream into the superheated liquid not withstanding whether or not wall nucleation sites were present. The body of the void would primarily consist of annular flow. In annular flow, the bulk of the liquid phase clings to the duct wall, and the vapor flowing faster in the center would strip droplets of liquid off the liquid layer which would further break up into dispersed minute particles. Most of the evaporation in the annular flow would come from the surface of the liquid layer which directly receives the heat input. Eventually, the liquid layer would be completely evaporated; then the liquid phase exists only in the form of minute dispersed particles which would evaporate either when impinging

on the superheated wall or by receiving heat from superheated vapor around them, or by "flashing" as they enter lower pressure environments.

In the bubble flow regime, the vaporization rate is

$$\Gamma_v = \int_{R_o}^{R_{max}} \frac{n(R_v,z,t)}{A} \, \rho_v \, 4\pi \, R_v^2 \, \dot{R}_v \, dR_v \qquad (22)$$

where

R_o = minimum radius of vapor bubbles

R_{max} = maximum radius of isolated vapor bubbles

n = number density distribution of vapor bubbles

R_v = radius of vapor bubble

$\dot{R}_v$ = rate of increase of vapor bubble radius

the number density would obey the equation

$$\frac{\partial n}{\partial t} + \frac{\partial}{\partial z}(nV_v) + \frac{\partial}{\partial R_v}(n\dot{R}_v) = 0 \qquad (23)$$

which is analogous to the Liouville's theorem in statistical mechanics. The "initial condition" of Eq. (23) is

$$n(R_o,z,t)\,\dot{R}_v\,(R_o,z,t) = S(z,t) \qquad (24)$$

$S(z,t)$ is the nucleation source strength in bubbles per unit time per unit length and is dependent on the system pressure, temperature (superheat) and deactivation history. The above equations appeared as equations (72),(74), (75), (76), (78), (79), (80) and (81) in [29] and their implications were illustrated in terms of

an example analyzing bubble growth from a single nucleating site. The velocity
of an isolated bubble can be estimated from first principles; however, since only
its initial growth period is of any interest (small bubbles), its velocity can be
approximated quite well by the mean flow velocity (or liquid velocity).

In the annular flow regime, because of the relatively large interfacial area,
thermodynamic equilibrium would be essentially realized except for a small amount
of temperature gradient required to sustain the conduction-convection heat trans-
fer in the liquid layer. Thus the vapor generation rate Γ_v can be calculated by
substituting Eq. (21) into Eq. (20). The velocity components however can be quite
different. The relation between them can be calculated from a formula derived
from Levy's "momentum exchange model" [49]:

$$(\frac{\rho_L}{\rho_v}) \frac{X^2}{\alpha} + \frac{1}{2}\left\{\frac{(1-2\alpha)}{(1-\alpha)^2}(1-X)^2 - 1\right\} = \text{const.} \quad (25)$$

where X is the mass flow quality defined as

$$X = \frac{\alpha\rho_v V_v}{\alpha\rho_v V_v + (1-\alpha)\rho_L V_L} \quad (26)$$

The constant on the right hand side is determined by matching (α, V_v, V_L) at the
head of the void to those resulting from the analysis of the propagation of the
void. The relations are somewhat different from Eq. (14), which implies a quasi-
steady state condition relative to the void. Rearranging Eq. (26), one can write

$$V_L = (\frac{\alpha}{1-\alpha})(\frac{X}{1-X})\frac{\rho_v}{\rho_L}V_v \quad (27)$$

Or, alternately,

$$V_v - V_L = \left[1 - (\frac{\alpha}{1-\alpha})(\frac{X}{1-X}) \frac{\rho_v}{\rho_L}\right] V_v \tag{28}$$

Above relations fully describe the required constitutive laws for the body of the annular flow. However, one must also have some description regarding the beginning of the annular flow or the head of the propagating void. In order to do this, it would be necessary to apply some judgement regarding the transition between bubble and annular flow regimes and perform self-consistent flow and energy balance analyses. Since available experimental evidence on sodium boiling suggests that void propagation proceeds without prior occurrence of bubble growth [43],[44], the results given in the previous section on "Void Propagation" applies. Thus, at the head of the void,

$$\Gamma_v = [\alpha\rho_v(V_v+v)]_{z=\ell} \delta(\ell) \tag{29}$$

where ℓ is the instantaneous location of the head of the void and $\delta(\ell)$ is the Dirac delta operator defined in terms of its operating characteristics:

$$\left.\begin{array}{l} \int\limits_{z<\ell} f(z) \delta(\ell) dz = 0 \\[2em] \int\limits_{z<\ell}^{z>\ell} f(z) \delta(\ell) dz = f(\ell) \\[2em] \int\limits_{z>\ell} f(z) \delta(\ell) dz = 0 \end{array}\right\} \tag{30}$$

Actual evaluation of Eq. (29) is contingent on the numerical solution of the following system of equations at $z=\ell$:

$$X'_\ell = \frac{(C_P)_L \, \theta}{h_{fg}} \tag{31}$$

$$X'_\ell = \alpha_\ell \left\{ \frac{(1-2\alpha_\ell) + \sqrt{(1-2\alpha_\ell)^2 + \alpha_\ell \left[2 \frac{\rho_L}{\rho_v} (1-\alpha_\ell)^2 + \alpha_\ell (1-2\alpha_\ell)\right]}}{2 (\frac{\rho_L}{\rho_v})(1-\alpha_\ell)^2 + \alpha_\ell (1-2\alpha_\ell)} \right\} \tag{32}$$

$$(V'_L + v) = (\frac{1-\alpha_\ell}{1-X'_\ell}) \sqrt{\frac{2g_c \, \theta}{\rho_L \, (dT/dp)_{sat}}} \tag{33}$$

$$\alpha_\ell \, \rho_v \, (V_v + v) = X'_\ell \, \rho_L \, (V'_L + v) \tag{34}$$

where

θ = superheat at the head of the void based on the pressure on its downstream side.

V'_L = liquid velocity ahead of the void.

Corresponding to the sudden generation of the vapor phase, there is also a rapid pressure drop across the head of the void:

$$\Delta P = \frac{\rho_L \, (V_L + v)^2}{2g_c} \left[(\frac{1 - X'_\ell}{1 - \alpha_\ell})^2 - 1 \right] \tag{35}$$

This information would be needed to determine θ. Eqs. (25) through (35) were given in [29] as Eqs. (44),(71), (102), (103), (104), (105), (106), (107), and (108).

The dispersed flow regime is reached when the duct wall is no longer covered with a continuous liquid film. The liquid phase is now finely dispersed in the bulk of vapor as individual droplets. The initial size of the droplet can be estimated from the critical Weber number:

$$\rho_v \frac{(V_v - V_L)^2 \delta}{\sigma} = 7.5 \tag{36}$$

where δ is the droplet diameter. $(V_v - V_L)$ may be taken to be the value at the point where the annular flow terminates. The number density of droplets can be determined from the void fraction:

$$N_L = (\frac{6}{\pi\delta^3}) \frac{\rho_L V_L - \rho_v V_v}{G - \rho_v V_v} \tag{37}$$

where N_L is the number of droplets per unit volume and G is the total mass velocity. Evaporation of the liquid droplets in a dispersed flow takes place simultaneously by three mechanisms:

(a) direct heating of those droplets impinging on the duct wall;

(b) heating of the droplets by the superheated vapor environment;

(c) flashing of the droplets as they are carried into lower pressure environments and thus becoming superheated.

The first two mechanism were considered together in a comprehensive study by Forslund and Rohsenow [45]. A derivation of the latter was due to Dougherty [46].

Consolidating these results, the total evaporative rate can be written as

$$\Gamma_v = \left(\frac{\pi \delta^3}{6}\right) \rho_L \left(\frac{\delta N_L}{\delta t}\right)_w + \frac{\pi N_L \delta^2}{h_{fg}} (q_v'' + q_{f\ell}'') \tag{38}$$

According to [45] and [47],

$$\left(\frac{\delta N_L}{\delta t}\right)_w = \frac{1.2 \, N_L^{2/3}}{D\delta(1-\Delta T_L^*)} \left[\frac{g_n \, \rho_v}{\mu_v (\pi \delta^3/6)^{1/3}}\right]^{1/4} \left[\left(\frac{K_v}{\rho_L \, C_P}\right) \left(\frac{\Delta T_w^*}{1 + \frac{7}{20} \Delta T_w^*}\right)\right]^{3/4} \tag{39}$$

is the rate of loss of droplets per unit volume due to wall impingement. D is the diameter of the duct. g_n is the acceleration field normal to the duct wall and may be due to the combined effects of gravity and swirl flow inserts. (μ_v, K_v, C_P) are vapor properties at the mean of the duct wall temperature, T_w, and the local saturation temperature, T_{sat}. ΔT_w^* and ΔT_L^* are the dimensionless wall and droplet superheats defined as

$$\Delta T_w^* = \frac{C_P (T_w - T_{sat})}{h_{fg}} \tag{40}$$

$$\Delta T_L^* = \frac{(C_P)_L (T_L - T_{sat})}{h_{fg}} \tag{41}$$

T_L is the temperature of the superheated liquid droplet and $(C_P)_L$ is its constant pressure specific heat. Droplet evaporation due to vapor superheat is [48]

$$\frac{\pi N_L \delta^2}{h_{fg}} q_v'' = \pi \left\{ 2 + 0.55 \left[\frac{(V_v - V_L)\delta}{\nu_v}\right]^{1/2} Pr^{1/3} \right\} \frac{\delta N_L K_v}{C_P} \Delta T_v^* \tag{42}$$

Here, the vapor properties (ν_v, K_v, C_p, Pr) should be determined at the mean of the vapor temperature (superheated), T_v, and the local saturation temperature. ΔT_v^* is the dimensionless vapor superheat

$$\Delta T_v^* = \frac{C_p(T_v - T_{sat})}{h_{fg}}$$ (43)

and the contribution from internal superheat of the liquid itself is [46]

$$\frac{\pi N_L \delta^2}{h_{fg}} \, q''_{f\ell} = \frac{3\pi \delta N_L K_L}{(C_p)_L} \left\{ \frac{(\Delta T_L^*)^2 - [(\frac{\delta_i}{\delta})^3 - 1]^2 \, (1-\Delta T_L^*)^2}{[(\frac{\delta_i}{\delta})^3 - 1] \, (1-\Delta T_L^*)} \right\}$$ (44)

K_L is the thermal conductivity of the liquid and δ_i is the initial droplet diameter. The number density of droplets satisfies the equation

$$\frac{\partial N_L}{\partial t} + \frac{\partial N_L V_L}{\partial t} + (\frac{\delta N_L}{\delta t})_w = 0$$ (45)

so long as the critical Weber number, Eq. (36), is not exceeded. Velocity slip of the droplets is governed by

$$a_L = (\frac{\partial}{\partial t} + V_L \frac{\partial}{\partial z}) V_L = \frac{3}{4} \frac{C_D \rho_v (V_v - V_L)^2}{\rho_L \delta} + g_z$$ (46)

where g_z is the gravitational acceleration along the duct. The critical Weber number condition can be rewritten as

$$\left| a_L - g_z \right| \frac{\rho_L \delta^2}{C_D \sigma} \geq 5.625 \tag{47}$$

If and when this condition is met, breakup would take place such that

$$\left. \begin{array}{c} (N_L)_{after} = 2 \, (N_L)_{before} \\[2em] (\delta)_{after} = 2^{-1/3} \, (\delta)_{before} \end{array} \right\} \tag{48}$$

Following the suggestion in [45], the drag coefficient in Eq. (45) is to be interpolated between two sets of experimental data:

$$C_D = C_{D2} + F \, (C_{D1} - C_{D2}) \tag{49}$$

where

$$F = \begin{cases} 0 & \text{if } a_L \leq 500 \text{ ft/sec}^2 \\ (a_L - 500)/5000 & \text{if } 500 < a_L < 5500 \\ 1.0 & \text{if } a_L \geq 5500 \end{cases} \tag{50}$$

C_{D1} and C_{D2} are shown graphically in Fig. 18.

The temperature of the superheated vapor, needed in Eq. (42), can be determined from the overall heat balance.

$$\frac{4}{\pi D^2} q = C_P \left[\frac{\partial}{\partial t} (\alpha \rho_v T_v) + \frac{\partial}{\partial z} (\alpha \rho_v V_v T_v) \right] + (\frac{\delta N_L}{\delta t})_w (\frac{\pi \delta^3}{6}) \, \rho_L \, h_{fg} (1 - \Delta T_L^*) \tag{51}$$
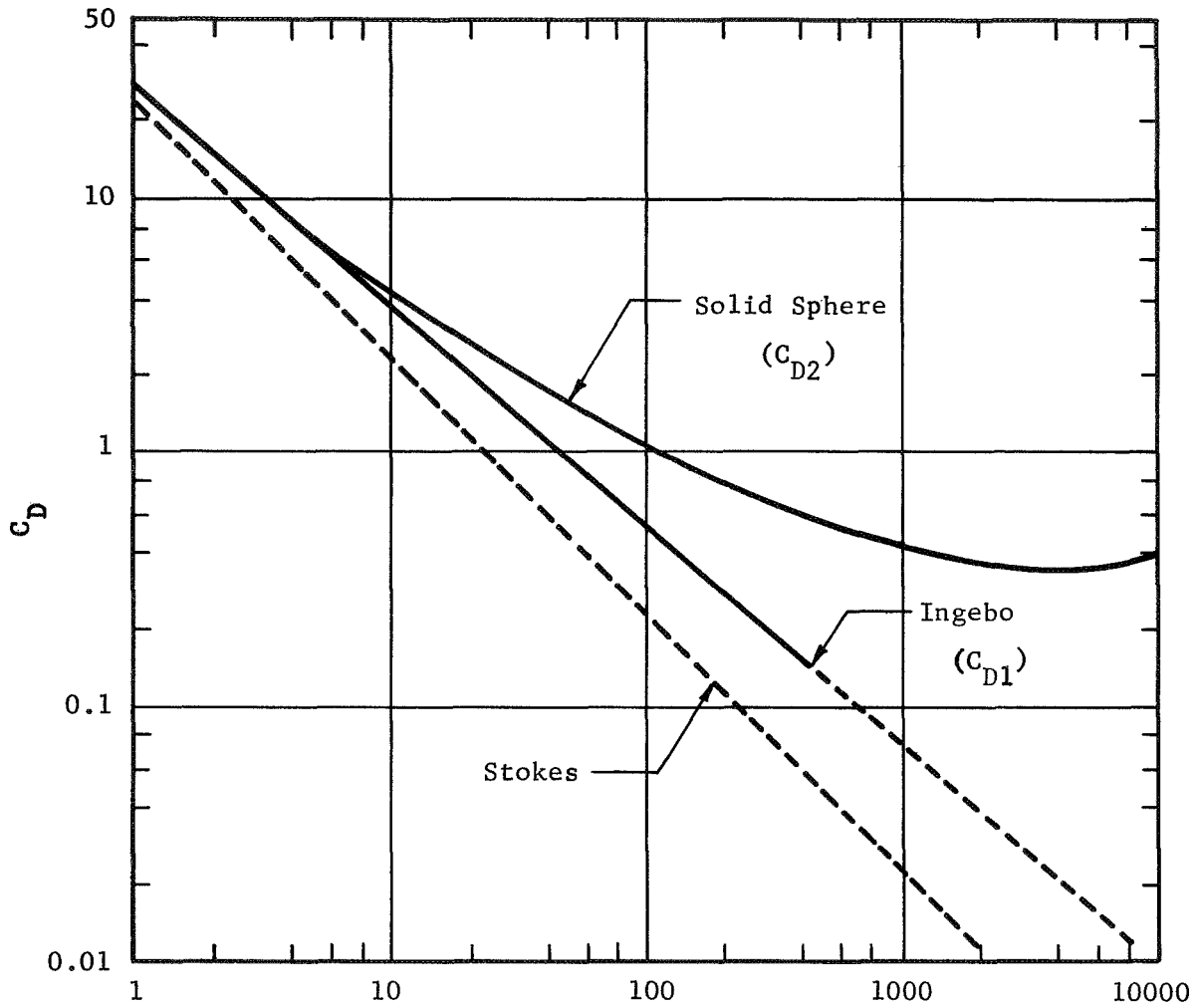
Fig. 18   Drag Coefficients

q is the heat input to the duct per unit length. Alternately, if the temperature of the duct wall is known, then

$$C_P \left[\frac{\partial}{\partial t} (\alpha \rho_v T_v) + \frac{\partial}{\partial z} (\alpha \rho_v V_v T_v) \right] = 0.076 \left(\frac{\rho_v V_v D}{\mu_v} \right)^{0.8} Pr^{0.4} \frac{K_v}{D^2} (T_w - T_v)$$

(52)

The void fraction is

$$\alpha = 1 - N_L \left(\frac{\pi \delta^3}{6} \right)$$

(53)

and the vapor-phase mass velocity is

$$\rho_v V_v = \frac{G - N_L \left(\frac{\pi \delta^3}{6} \right) \rho_L V_L}{1 - N_L \left(\frac{\pi \delta^3}{6} \right)}$$

(54)

G is the total mass velocity. Equation (51), in its reduced form, can also be used to determine the initial location of the dispersed flow regime; that is, at the beginning of the dispersed flow regime, the heat input to the duct is presumably balanced by the vaporizing heat of the impinging droplets:

$$\frac{4}{\pi D^2} q = \left(\frac{\delta N_L}{\delta t} \right)_w \left(\frac{\pi \delta^3}{6} \right) \rho_L h_{fg} \quad \text{at transition}$$

(55)

DISCUSSIONS AND CONCLUSIONS

An analytical description of the non-equilibrium forced convective boiling has been constructed from first principles. The chosen strategy here is to bring out the relevant and significant features of the overall physical system. In particular, emphasis is placed on the interplay of mass and heat transfer processes under non-equilibrium conditions for various flow structures.

The large degree of superheat required to initiate boiling nucleation in liquid metals is attributed to deactivation history in which subcooled liquid would flood and deactivate larger wall cavities. The subsequent superheat required to create vapor bubbles attached to the smaller cavities, which would overcome the surface tension and become a nucleus for continued vaporization, depends on the maximum pressure and subcooling during deactivation, micro-geometry of surface cavities, and amount of non-condensible gases. Because of the role of the micro-geometry of the surface, the phenomenon would take some form of statistical character. Available experimental data were obtained with test apparatus built of commercial grade materials; special surface treatments and exotic materials can cause substantial deviations from available experience. Also, the effects of heat flux and flow rate have not been explored. For liquids with relatively poor thermal conductivity, temperature gradient in the vicinity of nucleation would also exert some control over the incipience of boiling.

Subsequent to boiling incipience, relevant flow regimes which would have some significance in the dynamics of the thermo-hydraulic system are recognized to include bubble flow, annular flow, and dispersed flow.

In the early phase of bubble growth, proximity between neighboring bubbles may be assumed to be sufficiently far apart, so that one may make use of the analysis of the growth of an isolated single bubble. The latter has been treated previously. In the present work, a simplified method of computation was developed making possible rapid compilation of accurate growth rates for most fluids of interest. The growth rate of very small bubbles is inertially limited while that of the relatively larger ones is thermally limited. The growth rate is

largest for intermediate size bubbles. The range of bubble size for which the maximum growth rate approximately applies is wide enough to cover most situations of interest. For this reason the maximum growth rates have been compiled for water, potassium, and cesium.

Typically, the maximum growth rate is sufficiently rapid that upon incipient nucleation, one would expect the bubble to quickly grow into a large void, filling up most of the cross-section of the duct. Subsequent vaporization would then take place as release of superheat across the head of the void which would propagate upstream so that continued evaporation would no longer depend on the presence of nucleation site, nor would there be a significant region of bubble flow. The analysis of the void propagation was performed with the use of Levy's "momentum exchange model" applied to the moving void.

Downstream of the void, the annular flow regime prevails. Because of the abundance of interfacial areas, thermodynamic equilibrium is likely to be maintained. The vaporization rate can be readily computed from the energy equation provided the velocities of each phase is known. In the present work, a condition, which is equivalent to the determination of the slip velocity and is based on Levy's "momentum exchange model", was recommended.

Continued boiling due to heat addition would finally result in the dispersed flow. In this situation, it was necessary to consider three distinct mechanisms; namely, direct evaporization of those droplets impinging on the duct wall, evaporation of entrained droplets by heat received from superheated vapor, and "flashing" of the droplet because of its internal(liquid) superheat. The impingement rate was established according to a correlation which primarily attributes droplet diffusion to the transverse acceleration field. Therefore, the influence of swirl flow inserts can be directly evaluated. The transition condition between the annular flow and the dispersed flow was determined according to a heat balance between the wall heat flow and the evaporation heat of impinging droplets. The formula for heat transfer from the superheated vapor to the droplet was due to Tsubouchi and Sato, and the derivation of Dougherty was used to account for the flashing process.

The formulation of analysis proposed in the present work can be expected to yield meaningful numerical results. Such computations should be carried out for specific situations of immediate interest, then careful scrutiny and interpretation of the results obtained can render valuable inputs to the design technology of once-through liquid metal boilers as well as appropriate guidance to required research in this field.

From a rigorous scientific point of view, the experience in performing the studies for the present work has brought out the need to advance the present state of knowledge in several aspects.

(a) In the bubble flow regime, for situations in which the individual bubble size is no longer small in comparison with the distance between adjacent bubbles, the available information is largely empirical. It would be desirable to carry out a combined experimental and analytical study for this flow regime, emphasizing the determination of evaporation rate and phase-velocity components. Since this condition would become significant primarily when the bubble growth rate is slow relative to the convective velocity, the amount of liquid superheat, consequently the degree of non-equilibrium would not be substantial.

(b) Levy's "momentum exchange model" in the form used to analyze the annular flow regime in the present work, presumed either that the acceleration field is negligible or that the heat flux (or evaporation rate) is very high. For a situation in which the heat flux is relatively low, while there is a violent transient such as may be related to the rapid propagation of a central void, the "momentum exchange model" may not be valid. The required research should focus on the nature of interfacial momentum transport with a strong longitudinal acceleration field.

(c) Diffusion of droplets due to shear and turbulence in the dispersed flow regime is not yet amenable to quantitative analysis. This information is relevant to the transition condition from annular to dispersed flows and will also improve accuracy in the determination of the evaporative rate in the dispersed flow regime.

REFERENCES

1. Vohr, J. H. and Chiang, T., "A Review of Criteria for Predicting Incipient Nucleation in Liquid Metals and Ordinary Fluids", Technical Report MTI-69 TR45, prepared for NASA Headquarters, Washington, D.C. under Contract No. NASw-1705, Mechanical Technology Incorporated, Latham, N.Y. 12110, Nov., (1969).

2. Edwards, J. A. and Hoffman, H. W., "Superheat with Boiling Alkali Metals", Proc. Conf. on Application of High Temp. Instrumentation to Liquid-Metal Experiments, pp 515-534, ANL-7100, (1965).

3. Edwards, J. A. and Hoffman, H. W., "Incipient and Stable Boiling Superheat on a Surface Containing Cavities", ORNL-P-3083 Conf. 670909-1, (1966)

4. Holtz, R. E. and Singer, R. M., "Incipient Pool Boiling of Sodium", Communication to Editor, AICHE Journal, 14, No. 4, pp 654-656, (1968).

5. Holtz, R. E. and Singer, R. M., "On the Initiation of Pool Boiling in Sodium", Presented at Symposium on Heat Transfer on Fast Reactor Technology, 10th National Heat Transfer Conference, Philadelphia, (1968).

6. Marto, P. J., and Rohsenow, W. M., "Effects of Surface Conditions on Nucleate Pool Boiling of Sodium, J. Heat Transfer, ASME Series C, 88, No. 2, pp 196-204, (1966).

7. Lurie, H. and Noyes, R. C., "Boiling Studies for Sodium Reactor Safety; Part II Pool Boiling and Initial Forced Convection Task and Analyses", NAA-SR-9477, (1964).

8. Noyes, R. C. and Lurie, H., "Boiling Na Heat Transfer", Proc. of Third International Heat Transfer Conference, Vol. V, pp 92-100, Chicago, (1966).

9. Petukhov, B. S., Kovalev, S. A., Zhukov, V. M., "Study of Sodium Boiling Heat Transfer", Proc. of Third International Heat Transfer Conference, Vol. V, pp 80-91, Chicago (1966).

10. Shai, I. and Rohsenow, W. M., "The Mechanism of Nucleate Pool Boiling Heat Transfer to Sodium and the Criterion for Stable Boiling", MIT Dept. Mech. Eng. Report DSR76303-45, Jan. (1967).

11. Shai, I. and Rohsenow, W. M., "The Mechanism of the Stability Criterion for Nucleate Pool Boiling of Sodium, ASME Paper No. 68-WA/HT-15, Presented at Winter Annual Meeting, N.Y.C., (1968).

12. Chen, J. C., "Incipient Boiling Superheat in Liquid Metals", J. of Heat Trans. Series C, 90, No. 3, pp 303-312, (1968).

13. Logan, D., Landont, J., Boroczy, C., (Princ. Inv.), "Boiling Studies for Sodium Reactor Safety", Atomics International Annual Technical Progress Report - HEC Unclassified Programs, FY 1968, AI-AEC-12721,

REFERENCES (Continued)

14. Bond, J. A., Converse, G. L., "Vaporization of High-Temp. Potassium in Forced Convection at Saturation Temperatures of 1800° to 2100°F, NASA CR-843, July (1967).

15. Grass, G., Kottowski, H., Spiller, K. H., "Measurements of the Super-heating and Studies about Boiling Phenomena in Liquid Metals", Proceedings of International Conference on Safety of Fast Reactors, Aix-en Province, France, Sept. (1967).

16. LeGonidec, Rouvillios, Semeria, R., Lions, N., Robin, M. and Simon, "Experimental Studies on Sodium Boiling", Proc. of International Conference on Safety of Fast Reactors", Aix-en Province, France, Sept. (1967).

17. Pinchera, G. C., Tomassetti, G., Falzetti, L., Fornari, G., "Sodium Boiling Researches Related to Fast Reactor Safety", Trans. ANS Winter Meeting, Washington, D.C., Nov. (1968).

18. Pinchera, G. C., Tomassetti, G., Gambardella, G., Fanello, G. E., "Experimental Boiling Studies Related to Fast Reactor Safety", Proceedings of International Conference on Safety of Fast Reactors", Aix-en Province, France, Sept. (1967).

19. Smidt, D., Fette, P., Peppler, W., Schlechtendahl, E. G., and Schulteiss, G. F., "Problems of Sodium Boiling in Fast Reactors, Karlsruhe Report KFK 790, June (1968).

20. Logan, D., Landoni, J., Boroczy, C., (Principle Investigation), "Quarterly Technical Prog. Rep. AEC Unclassified Programs, Oct.-Dec., 1968, pp 59-64, AI-AEC-12777.

21. Chen, J. C., "Effect of Turbulent Flow on Incipient Boiling Superheat", Summaries of Presentations from First Meeting of the Technical Working Group on Liquid Metal Thermal Science, Brookhaven National Laboratory, Upton, N.Y., May (1969).

22. Holtz, R. E., "Sodium Superheat Studies at ANL", Summaries of Presentations from First Meeting of the Technical Working Group on Liquid-Metal Thermal Science, Brookhaven National Laboratory; Upton, N.Y., May (1969).

23. Holtz, R. E., "The Effect of the Pressure Temperature History Upon Incipient Boiling Superheats in Liquid Metals", Argonne National Laboratory Report ANL-7184, June, (1966).

24. Dwyer, O. E., "On Incipient Boiling Wall Superheats in Liquid Metals", Brookhaven National Laboratory Report 13NL-13039R Oct. 1968 (Revised March, 1969).

25. Hsu, Y. Y., "On the Size Range of Active Nucleation Cavities on a Heating Surface", Journal of Heat Transfer, ASME Trans. pp 207-216, August (1962).

REFERENCES (Continued)

26. Bergles, A. E., and Rohsenow, W. M., "The Determination of Forced Convection Surface Boiling Heat Transfer", Journal of Heat Transfer, No. 63-HT-22, pp 1-8, Sept. (1963).

27. Davis, E. J. and Anderson, G. H., "The Incipience of Nucleate Boiling in Forced Convection Flow", A.I.CH.E. Journal, Vol. 12, No. 4, pp 774-780, July (1966).

28. Chen, J. C., "Discussion of Incipient Boiling Superheat in Liquid Metals", Trans. ASME, J. Heat Transfer, 91 198-199 (1969).

29. Vohr, J. H., "Evaporative Processes in Superheated Forced Convective Boiling", Technical Report MTI-70TR15, prepared for NASA Headquarters, Washington, D.C., under Contract No. NASw-1705, Mechanical Technology Incorporated, Latham, N. Y. 12110, March (1970).

30. Lord Rayleigh, "On the Pressure Developed in a Liquid During the Collapse of a Spherical Cavity", Phil. Mag. S. 6, Vol. 34 No. 200, pp 94-98, August (1917)

31. Plesset, M. S. and Zwick, S. A., "The Growth of Vapor Bubbles in Superheated Liquids, J. Appl. Physics, Vol. 25, pp 493-500, (1954).

32. Forster, H. K. and Zuber, N., "Growth of a Vapor Bubble in a Superheated Liquid", J. Appl. Physics, Vol. 25, No. 4, pp 474-478, April, (1954).

33. Birkhoff, G.,Margulies, R. S. and Horning, W. A., "Spherical Bubble Growth", Physics of Fluids, Vol. 1, No. 3, pp 201-204, May-June, (1958).

34. Griffith, P., "Bubble Growth Rates in Boiling", Trans. ASME, Vol. 80, pp 721-727, (1958).

35. Scriven, L. E., "On the Dynamics of Phase Growth", Chemical Engineering Science, Vol. 10, Nos. 1/2, pp 1-12, (1959).

36. Bankoff, S. G., "Asymptotic Growth of a Bubble in a Liquid with Uniform Initial Superheat", Appl. Sci, Res., Section A, Vol. 12, pp 267-281, (1963-1964).

37. Theofanous, T., Biasi, L., Isbin, H. S., and Fauske, H., "A Theoretical Study on Bubble Growth in Constant and Time-Dependent Pressure Fields", Accepted for Publication in Chemical Engineering Science.

38. Bornhorst, W. J. and Hatsopoulos, G. N., "Bubble-Growth Calculation without Neglect of Interfacial Discontinuities", J. Applied Mech., pp 847-853, (1967).

39. Waldman, L. A. and Houghton, G., "Spherical Phase Growth in Superheated Liquids", Chemical Eng. Science, Vol. 20, pp 625-636, (1965).

REFERENCES (Continued)

40. Zuber, N. and Dougherty, D. E., "Liquid Metals Challenge to the Traditional Methods of Two-Phase Flow Investigation", Submitted for Presentation at the EURATOM Symposium of Two-Phase Flow Dynamics, Tech. Univ. of Eindhoven, Eindhoven Holland, Sept. 4-9 (1967).

41. Vohr, J. H., "Flow Patterns of Two Phase Flow - A Survey of Literature", Prepared for U. S. Atomic Energy Commission, Report TID-11514, Contract No. AT(30-3)-187, Task IX, Dec. (1960).

42. Von Glahn, Uwe H., and Polcyn, Richard P., "On the Effect of Heat Addition in the Empirical Correlation of Void Fractions for Steam-Water Flow", NASA Technical Note, NASA TN D-1440, November (1962).

43. Lewis, J. P., Groesbeck, D. E. and Christenson, H. H., "Tests of Sodium Boiling in a Single Tube-in-Shell Heat Exchanger Over the Range 1720° to 1980°F (1211 to 1355 K), NASA Technical Note, NASA TN D-5323, July, (1969).

44. Bond, J. A. and Converse, G. L., "Vaporization of High-Temperature Potassium in Forced Convection at Saturation Temperatures of 1800° to 2100°F", NASA Contractor Report, NASA CR-843, July (1967).

45. Forslund, R. P., Rohsenow, W. M., "Dispersed Flow Film Boiling", Trans. ASME, Journal of Heat Transfer, pp 399-406, November (1968).

46. Zuber, N. Dougherty, D. E., "Fluid Dynamics of Dispersed Two-Phase Vapor-Liquid Flow in Lubricant Films", Part I & II, MTI Technical Report MTI-68TR30, (1968); Also Appendix B of [29].

47. Baumeister, K. J., Hamill, T. D., and Schoessow, G. J., "A Generalized Correlation of Vaporization Times of Drops in Film Boiling on a Flat Plate", US-AICHE No. 120, 3rd International Heat Transfer Conference and Exhibit, August 7-12, (1966).

48. Tsubouchi and Sato, "Heat Transfer between Single Particles and Fluids in Relative Forced Convection", Chemical Engineering Progress Symposium Series, Vol. 55, (1960).

49. Levy, S., "Steam Slip-Theoretical Prediction from Momentum Model", Journal of Heat Transfer, ASME Trans., Series C, Vol. 82, 113-124 (1960).

Distribution List For Reports
Study of Thermo-Hydraulic Oscillations in Boiling
Systems Employing Liquid Metal Working Fluids
Contract No. NASW-1705
Mechanical Technology Incorporated
968 Albany-Shaker Road
Latham, New York 12110

ADDRESSEE	NUMBER OF COPIES	ADDRESSEE	NUMBER OF COPIES
Jet Propulsion Laboratory 4800 Oak Grove Drive Pasadena, California 91103 Attn: G.M. Kikin, Mail Stop 122-103	1	Aerojet-General Corporation Von Karman Center P.O. Box 296 Azusa, California 91702 Attn: Librarian	2
General Electric Company Knolls Atomic Power Laboratory Schenectady, New York Attn: G. Halsey	1	University of Michigan Department of Chemical and Metallurgical Engineering Ann Arbor, Michigan 48105 Attn: R.E. Balzhieser	2
General Electric Company Knolls Atomic Power Laboratory Schenectady, New York Attn: J. Carr	1	Massachusetts Institute of Technology Cambridge, Massachusetts 02139 Attn: W.M. Rohsenow	2
General Electric Company Knolls Atomic Power Laboratory Schenectady, New York Attn: Library	1	New York University Dept. of Mechanical Engineering New York, New York 10003 Attn: N. Zuber	10
General Electric Company Missiles and Space Power Section Cincinnati, Ohio 45215 Attn: M.A. Zipkin	1	New York University Dept. of Mechanical Engineering New York, New York 10003 Attn: Library	2
General Electric Company Missiles and Space Power Section Cincinnati, Ohio 45215 Attn: J.R. Peterson	2	Department of the Air Force Air Force Aero Propulsion Laboratory Wright-Patterson Air Force Base, Dayton, Ohio 45433 Attn: C.H. Armbruster	1
General Electric Company 175 Courtner Avenue San Jose, California 95125 Attn: S. Levy	2	Department of the Air Force Air Force Aero Propulsion Laboratory Wright-Patterson Air Force Base, Dayton, Ohio 45433 Attn: J.W. Zmurk	1
General Electric Company 175 Courtner Avenue San Jose, California 95125 Attn: F.E. Tippets	2	A. Research Manufacturing Company 9851 Sepulveda Boulevard Los Angeles, California 90009 Attn: F.E. Carroll	2
General Electric Company 175 Courtner Avenue San Jose, California 95125 Attn: K. Cohen, Manager APO	1	A. Research Manufacturing Company 9851 Sepulveda Boulevard Los Angeles, California 90009 Attn: P.J. Berenson	1
General Electric Company 310 DeGuigne Drive Sunnyvale, California 95125 Attn: W.G. Meinhardt	1	Columbia University Department of Chemical Engineering New York, New York 10027 Attn: C.F. Bonilla	2
AiResearch Manufacturing Company 402 South 36 Street Phoenix, Arizona 85034 Attn: R. Gruntz	1	NASA Scientific & Technical Information Facility P.O. Box 33 College Park, Maryland 20740	Reproducible Copy
AiResearch Manufacturing Company 402 South 36 Street Phoenix, Arizona 85034 Attn: Library	2	M.J. SAMES, LIBRARIAN NEW DEPARTURE-HYATT BEARINGS DIV. 2509 HAYES AVE. SANDUSKY, OHIO 44870	
Geoscience Ltd. 410 South Cedros Avenue Solana Beach, California 92075 Attn: H.F. Poppendiek	2	General Electric Company Knolls Atomic Power Laboratory Schenectady, New York 12305 Attn: O. Jones	1
TRW Systems Group One Space Park Redondo Beach, California 90278 Attn: S.M. Zivi	1	NASA Lewis Research Center 21000 Brookpark Road Cleveland, Ohio 44135 Attn: M. Gutstein Mail Stop 500-201	1
TRW Systems Group One Space Park Redondo Beach, California 90278 Attn: L.G. Neal	1		

Study of Thermo-Hydraulic Oscillations in Boiling
Systems Employing Liquid Metal Working Fluids
Contract No. NASW-1705
Mechanical Technology Incorporated
968 Albany-Shaker Road
Latham, New York 12110

ADDRESSEE	NUMBER OF COPIES	ADDRESSEE	NUMBER OF COPIES
NASA Headquarters Code RNP Washington, D.C. 20546 Attn: S.V. Manson	2	NASA Lewis Research Center 21000 Brookpark Road Cleveland, Ohio 44135 Attn: U.H. Von Glahn, Mail Stop 2120	1
NASA Headquarters Code RNP Washington, D.C. 20546 Attn: J.J. Lynch	1	NASA Lewis Research Center 21000 Brookpark Road Cleveland, Ohio 44135 Attn: R.G. Dorsch, Mail Stop 2123	4
NASA Headquarters Code RNP Washington, D.C. 20546 Attn: F. Schulman	1	NASA Lewis Research Center 21000 Brookpark Road Cleveland, Ohio 44135 Attn: J.P. Lewis, Mail Stop 2121	1
NASA Lewis Research Center 21000 Brookpark Road Cleveland, Ohio 44135 Attn: B. Lubarsky, Mail Stop 9200	1	NASA Lewis Research Center 21000 Brookpark Road Cleveland, Ohio 44135 Attn: R.W. Graham, Mail Stop 2142	1
NASA Lewis Research Center 21000 Brookpark Road Cleveland, Ohio 44135 Attn: R.E. English, Mail Stop 9200	1	NASA Lewis Research Center 21000 Brookpark Road Cleveland, Ohio 44135 Attn: Y. Hsu, Mail Stop 2142	1
NASA Lewis Research Center 21000 Brookpark Road Cleveland, Ohio 44135 Attn: T.A. Moss, Mail Stop 9220	1	NASA Lewis Research Center 21000 Brookpark Road Cleveland, Ohio 44135 Attn: V.H. Gray, Mail Stop 2121	1
NASA Lewis Research Center 21000 Brookpark Road Cleveland, Ohio 44135 Attn: R.N. Weltmann, Mail Stop 9232	2	Argonne National Laboratory Argonne, Illinois 60439 Attn: Library Services, Department 203-CE125 Report Section	3
U.S. Atomic Energy Commission Washington, D.C. 20545 Attn: N. Grossman, Code DRD&T	1	Oak Ridge National Laboratory Oak Ridge, Tennessee 37830 Attn: A.P. Fraas	1
U.S. Atomic Energy Commission Washington, D.C. 20545 Attn: C. Johnson, Code SNS	1	Oak Ridge National Laboratory Oak Ridge, Tennessee 37830 Attn: W.H. Hoffman	1
U.S. Atomic Energy Commission Washington, D.C. 20545 Attn: G. Leighton, Code SNS	1	Oak Ridge National Laboratory Oak Ridge, Tennessee 37830 Attn: Library	1
U.S. Atomic Energy Commission Washington, D.C. 20545 Attn: R. Scroggins, Code DRD&T	1	Los Alamos Scientific Laboratory Los Alamos, New Mexico 87544 Attn: R.S. Thurston	2
U.S. Atomic Energy Commission Washington, D.C. 20545 Attn: S. Salewitz, Code SNPO	1	Los Alamos Scientific Laboratory Los Alamos, New Mexico 87544 Attn: Library	1
Brookhaven National Laboratory Upton, New York 11973 Attn: D.H. Gurinsky	1	Jet Propulsion Laboratory 4800 Oak Grove Drive Pasadena, California 91103 Attn: D.R. Bartz, Section 383	1
Brookhaven National Laboratory Upton, New York 11973 Attn: O.E. Dwyer	1	Jet Propulsion Laboratory 4800 Oak Grove Drive Pasadena, California 91103 Attn: J.P. Davis, Section 383	1
Brookhaven National Laboratory Upton, New York 11973 Attn: J.C. Chen	1		
Brookhaven National Laboratory Upton, New York 11973 Attn: L.M. Shotkin	1		

MTI-5603

MECHANICAL TECHNOLOGY INCORPORATED

968 ALBANY-SHAKER ROAD, LATHAM, NEW YORK 12110   AREA CODE 518   PHONE 785-2211